Adenoviral Delivery of the CIITA Transgene Induces T-Cell-Mediated Killing in Glioblastoma Organoids

Ilaria Salvato[1,2,3,*], Eliane Klein[1,3,*], Aurélie Poli[4], Mahsa Rezaeipour[1], Luca Ermini[1], Bakhtiyor Nosirov[1,5], Anuja Lipsa[1], Anais Oudin[1], Virginie Baus[1], Gian Mario Dore[2], Antonio Cosma[6], Anna Golebiewska[1], Simone P. Niclou[1,3,§], Antonio Marchini[2,7,8,§].

[1]NORLUX Neuro-Oncology Laboratory, Department of Cancer Research, Luxembourg Institute of Health (LIH), Luxembourg;

[2]Laboratory of Oncolytic Virus Immuno-Therapeutics (LOVIT), Department of Cancer Research, Luxembourg Institute of Health (LIH), Luxembourg;

[3]Department of Life Sciences and Medicine, Faculty of Science, Technology and Medicine (FSTM), University of Luxembourg, Luxembourg;

[4]Neuro-Immunology Group, Department of Cancer Research, Luxembourg Institute of Health (LIH), Luxembourg;

[5]Multiomics Data Science Research Group, Department of Cancer Research, Luxembourg Institute of Health (LIH), Luxembourg;

[6]National Cytometry Platform, Translational Medicine Operation Hub, Luxembourg Institute of Health, Esch-sur-Alzette, Luxembourg;

[7]Laboratory of Oncolytic Virus Immuno-Therapeutics, German Cancer Research Center, Heidelberg, Germany.

[8]Current address: European Commission, Joint Research Centre (JRC), Geel, Belgium;

* Equal contribution

[§] Co-senior authors and corresponding authors

WORD COUNT (Excluding References): 10.989

ABSTRACT

The immunosuppressive nature of the microenvironment poses significant challenges in developing effective immunotherapies against glioblastoma (GBM). Enhancing immune-mediated responses is a prerequisite for a successful therapy. Here, we present a cancer gene therapy approach utilizing a replication-deficient adenovirus (AdV) armed with the Class II Major Histocompatibility Complex (MHC-II) Transactivator *CIITA* gene (Ad-CIITA) to induce antigen-presenting properties in GBM cells. Successful induction of MHC-II molecules at the cell membrane was achieved in infected GBM cell lines and primary human GBM organoids. Infection

with an AdV carrying a mutant form of *CIITA* resulted in cytoplasmic accumulation of CIITA without subsequent MHC-II expression. Intriguingly, both wild-type and mutant Ad-CIITA triggered prominent immune-mediated tumor cell death in a co-culture system with primary human GBM organoids, suggesting a partially MHC-II-independent process. We further show that the observed cancer cell killing requires the presence of T-cells and direct contact between GBM and immune cells. Overall, these findings highlight that AdV-mediated *CIITA* delivery enhances T-cell-mediated immunity against GBM, the precise mechanism of which remains to be elucidated.

KEYWORDS

Adenovirus/Gene therapy/Glioblastoma/MHC-II/Tumor Organoids

INTRODUCTION

Malignant brain tumors including glioblastoma (GBM) remain a major clinical and scientific challenge. In GBM patients the median overall survival is limited to 12-15 months after tumor diagnosis (Ostrom, Cioffi et al. 2021). The immunosuppressive tumor microenvironment (TME) as well as systemic immunosuppression pose multiple challenges to novel immunotherapies. GBMs recruit immunosuppressive cell types such as tumor-associated microglia and macrophages (TAMs) and regulatory T-cells (Tregs), while only a limited number of T-cells are present, the latter often displaying exhaustion markers that inhibit immune cell function (Quail and Joyce 2017, Woroniecka, Chongsathidkiet et al. 2018, Pires-Afonso, Niclou and Michelucci 2020). GBM tumors may also downregulate the expression of major histocompatibility complex (MHC) molecules, surface glycoproteins that play a central role in presenting cancer-derived antigens to the immune system (Burster, Gärtner et al. 2021).

Several immunotherapeutic approaches have been investigated for the treatment of GBM, including immune checkpoint inhibitors, vaccines, adoptive cell therapy, as well as virus-based therapy, utilizing oncolytic viruses and replication-deficient virus-mediated cancer gene therapy (Agosti, Zeppieri et al. 2023). Despite promising results in preclinical studies, these treatments, whether tested individually or in combination with standard care, have so far failed to translate in clinically meaningful outcomes for GBM patients (Rainov 2000, Immonen, Vapalahti et al. 2004, Weller, Butowski et al. 2017, Narita, Arakawa et al. 2019, Cloughesy, Brenner et al. 2020, Cloughesy, Petrecca et al. 2020, Reardon, Brandes et al. 2020, Lim, Weller et al. 2022, Liau, Ashkan et al. 2023, Omuro, Brandes et al. 2023). The discrepancy between clinical and preclinical results can be largely attributed to the inadequacy of efficacy studies based on oversimplified preclinical models not recapitulating the complex biology of GBM tumors.

68 Replication-deficient adenoviruses (AdVs) have demonstrated safety and tolerability as gene
69 therapy and vaccination vectors, e.g. in the treatment of various cancer types, including GBM.
70 Current GBM treatments using AdV derived vectors focus on the delivery of herpes simplex virus
71 (HSV) thymidine kinase (TK), p*53*, interleukin (IL)-12, interferon (IFN)-β, and a chimeric death
72 receptor (VB-111) (Banerjee, Nunez et al. 2021).
73 A promising approach is to arm non-lytic AdV vectors with novel therapeutic transgenes, able to
74 boost immune responses against GBM. Class II Major Histocompatibility Complex Transactivator
75 (CIITA) is the master regulator of MHC class II (MHC-II) molecules, expression of which is largely
76 limited to professional antigen presenting cells (APCs) (Forlani, Shallak et al. 2023). Upon
77 expression and translocation to the nucleus, CIITA acts as a non-DNA binding transcriptional
78 coactivator by interacting with the enhanceosome complex. This complex consists of several
79 constitutively-expressed DNA-bound factors preassembled at MHC-II promoters (Leon Machado
80 and Steimle 2021). CIITA then nucleates various transcription factors and chromatin modifiers
81 necessary to activate the transcription of the cell surface "classical" human leukocyte antigen
82 (HLA)-DR, HLA-DP and HLA-DQ glycoproteins, which physically present antigens to $CD4^+$ T helper
83 cells, as well as HLA-DM, HLA-DO and invariant chain (Ii) molecules, which are involved in
84 intracellular antigen processing (Leon Machado and Steimle 2021). Previous work on carcinoma
85 cell lines (Sartoris, Valle et al. 1998, Hillman, Kallinteris et al. 2003, Mortara, Castellani et al. 2006,
86 Thompson, Dissanayake et al. 2006, Palma, Duangkhae et al. 2017), and more recently on murine
87 glioma cells (Celesti, Gatta et al. 2023), found that ectopic stable expression of CIITA can
88 transform tumor cells into MHC-II-positive cells with enhanced antigen processing and
89 presentation capabilities. In these models, CIITA-transfected/infected MHC-II-positive cells were
90 capable of priming and activating $CD4^+$ T helper cells, resulting in effective tumor rejection or
91 growth retardation in mice with subcutaneous tumors (Hillman, Kallinteris et al. 2003, Meazza,
92 Comes et al. 2003, Thompson, Dissanayake et al. 2006, Frangione, Mortara et al. 2010, Bou Nasser
93 Eddine, Forlani et al. 2017, Palma, Duangkhae et al. 2017, Celesti, Gatta et al. 2023).
94 Here, we engineered a replication-deficient serotype 5 adenovirus (AdV) with the *CIITA* transgene
95 ("Ad-CIITA") with the aim of converting infected primary human GBM organoids into "surrogate"
96 APCs. The primary objective was to design a gene therapy that would enable the infected tumor
97 cells to prime and activate T helper cells, thereby fostering antitumor immune responses. A
98 second objective was to establish an advanced human GBM organoid system, based on primary
99 organoids co-cultured with human immune cells, to assess the functional impact of the virus in a
100 complex model system. We find that in our model system, AdV-mediated delivery of the *CIITA*
101 transgene effectively induces cancer cell death in the presence of immune cells. While the exact

102 mechanism remains to be elucidated, our data suggest that the effect is at least partially
103 independent of MHC-II expression.

104 **RESULTS**

105 **MHC-II expression in GBM is limited to non-neoplastic cells of the tumor microenvironment.**

106 To assess the diversity of MHC-II molecules in GBM, we examined gene expression profiles at bulk
107 and single cell level in patient tumors and preclinical models. At bulk RNA level, expression of
108 *CIITA* and genes coding for MHC-II antigen presenting molecules (*HLA-DQA1*, *HLA-DQB1*, *HLA-*
109 *DRA, HLA-DRB1, HLA-DRB5)* was higher in GBM patient tumors than in normal brain tissue (**Fig.**
110 **1A**). However, analysis of single cell RNA-seq profiles of GBM patient tumors revealed that tumor
111 cells do not express *CIITA* nor genes encoding for MHC-II antigen processing (*CD74*, *HLA-DMA*,
112 *HLA-DOA*) and presentation (*HLA-DQA1*, *HLA-DQB1*, *HLA-DRA, HLA-DRB1, HLA-DRB5)* (**Fig. 1B**).
113 High expression of these genes was detected in immune cells of the tumor microenvironment,
114 explaining the high transcript levels observed by bulk RNA-seq. The highest MHC-II expression was
115 detected in well-known APCs, including dendritic cells, macrophages, microglia, and B cells (**Fig.**
116 **1B**). Limited cancer cell expression of MHC-II genes was confirmed in GBM patient-derived
117 orthotopic xenografts (PDOXs), where bulk RNA-seq profiles across 28 PDOXs showed low
118 expression of human genes involved in MHC-II antigen processing and presentation and
119 moderately high levels of enhanceosome-associated genes (**Fig. 1C**). Similar expression profiles
120 were seen in human GBM cell lines, including adherent and 3D sphere cultures of GBM stem-like
121 cells (GSCs) (**Supplementary Fig. 1A**). Only the U87 cell line presented high expression of certain
122 MHC-II associated genes (e.g., *CD74*, *HLA-DPA1*, *HLA-DRA*, *HLA-DRB4*, and *HLA-DRB5*).
123 Interestingly, the genes associated with the MHC-II enhanceosome complex (*CREB1*, *NFYA*, *NFYB*,
124 *NFYC*, *RFX5*, *RFXANK*, and *RFXAP)* showed sustained expression throughout patient tumors, PDOX
125 and cell lines (**Supplementary Fig. 1A**), suggesting that GBM cells have the capacity to express
126 MHC-II molecules upon activation of the MHC-II master regulator CIITA. Moreover, most of the
127 preclinical models exhibited transcriptional expression of the Coxsackie and Adenovirus Receptor
128 (*CXADR*), the specific receptor for AdV serotype 5, as well as the integrin αvβ5 necessary for AdV
129 infection (*ITGAV* and *ITGB5*) (Nemerow and Stewart 1999) (**Fig. 1C, Supplementary Fig. 1A**). This
130 observation implies that GBM tumor cells are likely to be susceptible to AdV infection, highlighting
131 the suitability of non-lytic AdVs for cancer gene therapy applications targeting GBM.
132 Next, we assessed the presence of MHC-II proteins at the cell surface of GBM cells by flow
133 cytometry. The majority of GBM cells showed no MHC-II protein at the cell surface under regular
134 culture conditions (**Fig. 1D, Supplementary Fig.1B**). Out of 10 GBM cell lines analyzed, only U87

135 and BG5 cells showed some positive cells (18.7% and 10.8% respectively). Interestingly, IFN-γ
136 cytokine stimulus did not activate MHC-II expression in GBM cells, except for U87, BG5, and
137 T16NS (**Fig. 1D**).
138 In summary, we confirmed that MHC-II molecules are largely absent from GBM tumor cells but
139 are expressed in tumor-associated APCs. Based on the presence of transcripts of the MHC-II
140 enhanceosome complex, ectopic expression of CIITA appears as a valid strategy to deliver MHC-II
141 molecules at the cell membrane. Moreover, the expression of the necessary AdV receptor and cell
142 adhesion molecules confers infectivity to GBM cells to serotype 5 AdVs.

143 **Human GBM stem-like cells infected with Ad-CIITA express CIITA and present MHC-II molecules**
144 **at the cell surface.**

145 To convert MHC-II-negative GBM tumor cells into MHC-II-positive cells with APC-like properties,
146 we generated a replication-deficient AdV carrying the wild-type *CIITA* gene (Ad-CIITA) (**Fig. 2A**).
147 The serotype 5 AdV backbone is widely employed in cancer gene therapy for its ability to
148 efficently transduce large transgenes (up to 8 Kbases) in a vast range of cell and tissue types,
149 including GBM. Importantly, AdVs can infect both proliferating and quiescent cells and their DNA
150 does not integrate into the host genome, but rather remains episomally in the host nucleus,
151 precluding the risk of insertional mutagenesis (Bulcha, Wang et al. 2021). Three different AdV
152 control vectors were generated, harboring either: i) no transgene (Ad-null); ii) a green fluorescent
153 protein (GFP)-encoding transgene (Ad-GFP); or (iii) a mutated *CIITA* transgene (Ad-CIITA mutant)
154 (**Fig. 2A**). The latter was newly generated in our laboratory, carrying a novel missense point
155 mutation (guanine-to-adenosine) (**Supplementary Fig. 2A**) that translated into a full-length CIITA
156 protein with a glycine (G) to arginine (A) substitution at amino acid position 1088 (**Supplementary**
157 **Fig. 2B**). We found that this mutation impaired the translocation of the MHC-II transactivator to
158 the cell nucleus (**Supplementary Fig. 2C**).
159 To determine optimal viral infection, we infected mouse glioma GL261 cells at various
160 multiplicities of infection (MOIs) and assessed MHC-II expression via flow cytometry at 72 hours
161 post-infection. The Ad-CIITA vector successfully delivered the human *CIITA* transgene into the
162 murine cell line, leading to a dose-dependent increase in IA-IE (MHC-II molecules) levels at the cell
163 membrane compared to non-infected controls (**Supplementary Fig. 2D**). Specifically, at a virus
164 MOI of 50, GL261 tumor cells expressed the CIITA transactivator at both mRNA and protein levels
165 (**Supplementary Fig. 2E**). Notably, the expression of IA-IE (MHC-II) molecules peaked at 72 hours
166 post-infection, with nearly all tumor cells displaying them at the cell membrane (**Supplementary**
167 **Fig. 2F**).

168 Next, we assessed AdV-mediated expression of MHC-II molecules in human 3D GSC lines (P3NS
169 and T16NS) by infecting the cells with a virus MOI of 50. High *CIITA* mRNA (**Fig. 2B**) and protein
170 (**Fig. 2C**) were detected at 72 hours post-infection with both Ad-CIITA and Ad-CIITA mutant
171 viruses. Since only wild-type CIITA translocates to the nucleus (**Supplementary Fig. 2C**), HLA-DRα
172 mRNA and protein were only detected in GBM cells infected with Ad-CIITA but not with Ad-CIITA
173 mutant virus (**Fig. 2B-C**). Surface MHC-II molecules were confirmed by flow cytometry using a pan
174 antibody targeting all surface MHC-II antigen presenting molecules (HLA-DR/DP/DQ epitopes)
175 (**Fig. 2D**). As expected, GBM cells infected with Ad-CIITA mutant virus did not display MHC-II
176 molecules at the cell surface (**Fig. 2D**). In summary, we show efficient infection of human GBM
177 cells leading to MHC-II molecules at the cell membrane, a necessary requirement for functional
178 antigen presentation. Moreover, a mutant CIITA construct has been generated which allows to
179 effectively distinguish the effects of nuclear versus non-nuclear CIITA expression.

180 **Infection with Ad-CIITA induces MHC-II expression in human primary GBM organoids.**

181 Following the results in adherent and 3D GBM cell lines, we next determined the efficacy of Ad-
182 CIITA virus in primary GBM organoids, obtained from mechanical dissociation of patient tissue,
183 followed by serial transplantation as PDOXs (Golebiewska, Hau et al. 2020). Following our well-
184 established protocol (Oudin, Baus et al. 2021), GBM organoids of uniform size can be cultured
185 short term *ex vivo* without repeatable passaging *in vitro*, which allows for preservation of complex
186 molecular features and a proliferative rate similar to *in vivo* tumors. We selected three GBM (P3,
187 T16 and T188) representing tumors with classical genetic and epigenetic features, including gain
188 of Chr7 and loss of Chr10 (**Table S1**).
189 To determine the optimal viral MOI, we infected P3 organoids with increasing MOI of Ad-CIITA for
190 up to 7 days post-infection. An MOI between 25 and 100 led to strong ectopic expression of CIITA
191 and HLA-DRα at 72 hours post-infection (**Fig. 3A**). GBM organoids infected with Ad-CIITA at MOI
192 75 exhibited a tissue structure comparable to that of non-infected GBM organoids, albeit with a
193 somewhat lower cell density (**Fig. 3B**). Again, HLA-positive cells were only detected in Ad-CIITA-
194 infected cells (**Fig. 3B** lower panel). Flow cytometry confirmed that Ad-CIITA infection successfully
195 translated into expression of MHC-II molecules at the cell membrane (**Fig. 3C**).
196 To evaluate the cytotoxicity of virus infection in primary GBM cells, dsRed-expressing P3
197 organoids were infected with Ad-CIITA or control viruses (Ad-null and Ad-CIITA mutant) at
198 increasing MOIs and monitored real-time with the Incucyte S3 live cell imaging system. Tumor cell
199 viability was assessed by the dsRed fluorescence intensity signal over time. Consistent with
200 previous studies showing that first-generation AdV vectors can lead to cell cycle arrest at elevated

201 MOIs (Zheng, Goldsmith et al. 2000), AdV infected organoids exhibited a dose-dependent
202 reduction in growth rate compared to non-infected organoids (**Fig. 3D**). This effect appeared more
203 evident with the wild-type Ad-CIITA vector (**Fig. 3D**). However, viral infection per se did not result
204 in cell death, as deduced from the dsRed fluorescence signal (**Fig. 3D**) and the H&E stained
205 sections (**Fig. 3B**). Similar results were seen in T16 GBM organoids, while in T188 organoids the
206 proliferation rate did not seem to be affected by viral infection (**Supplementary Fig. 3**).
207 In conclusion, our AdV-CIITA constructs effectively infect primary GBM organoids with only a
208 small impact on tumor growth. Robust MHC-II expression is obtained with Ad-CIITA, but not with
209 the control Ad-null or Ad-CIITA mutant vectors.

210 **Ad-CIITA triggers immune-mediated GBM tumor cell death primarily mediated by $CD3^+$ T-cells.**

211 To evaluate the potential of CIITA-expressing human GBM to elicit adaptive immune responses,
212 we established a protocol involving the co-culture of virally-infected primary GBM organoids with
213 allogenic peripheral blood mononuclear cells (PBMCs). PBMCs were obtained from healthy donors
214 or from partially HLA-matched donors (**Fig. 4A**). For efficient monitoring and quantification of
215 viability, we employed fluorescently-labeled GBM organoids, either through dsRed expression (P3
216 and T16) or labeling with cytolight rapid red dye (T188). Prior to adding immune cells, GBM
217 organoids were infected with Ad-CIITA for 72 hours, at MOI 75 (P3 and T188) or MOI 25 (T16) to
218 allow adequate MHC-II surface expression. Control GBM organoids were left uninfected or
219 infected with the control viruses Ad-null or Ad-CIITA mutant. Ad-null-infected and non-infected
220 GBM organoids enabled assessment of viral backbone intrinsic toxicity and immunogenicity in co-
221 culture conditions. GBM organoids were then co-cultured with non-labeled PBMCs or purified
222 individual immune cell populations of interest ($CD3^+$, $CD4^+$, $CD8^+$ T-cells) at different
223 target:effector (T:E) ratios (1:1, 1:5, 1:10) for up to 6 days. The purity of PBMCs and isolated cell
224 types were assessed by flow cytometry before co-culture (**Supplementary Fig. 4A, Table S2**). Co-
225 cultures were continuously monitored using the Incucyte S3 live cell imaging system (**Fig. 4A**) and
226 tumor cell death was monitored by tracking the decline in dsRed signal over time.
227 Based on previous tumor-immune cell co-culture studies (Zhou, Lieshout et al. 2022), we decided
228 to first use immune cells from healthy human donors for our co-culture setup. In the absence of
229 immune cells, P3 GBM organoids retained their structure, their proliferation being slightly
230 affected by viral infection (Ad-null) and further by CIITA expression (Ad-CIITA) (**Fig. 4B**), in line
231 with the experiments without co-culture conditions shown in **Fig. 3D**. Upon the addition of
232 allogenic PBMCs, we observed a pronounced organoid disruption and tumor cell killing in Ad-
233 CIITA-infected organoids (86,5%±10,2), contrasting with a lower effect in Ad-null-infected

234 organoids (42,2%±7,3) (**Fig. 4B, Video S1**). Throughout the text, the reported percentages in
235 parentheses represent a reduction in dsRed signal compared to non-infected controls at the end-
236 point of the co-culture. These findings imply that the induction of PBMC killing capacity is
237 primarely associated with the expression of CIITA by the tumor cells rather than solely through
238 the acquired immunogenicity linked to AdV infection itself.
239 To further investigate the association between the observed killing and MHC-II surface
240 expression, we conducted co-cultures using allogenic PBMCs and organoids infected with the Ad-
241 CIITA mutant virus. Interestingly, the Ad-CIITA mutant also led to robust tumor cell killing in the
242 presence of PBMCs (78,3%±21,7) (**Fig 4B, Video S1**). This was unexpected as we have shown that
243 this construct did not induce MHC-II molecules expression (**Fig. 2B-C**). Similar outcomes were
244 obtained in T16 GBM organoids at different MOIs (25 and 75), where no cell death was observed
245 in uninfected or Ad-null-infected T16 organoids. Pronounced tumor cell death was induced by Ad-
246 CIITA and again, though to a lesser extent, by Ad-CIITA mutant (**Supplementary Fig. 4B**). These
247 data suggest that CIITA expression potentiates the immunogenicity of GBM organoids for
248 alloreactive PMBCs, potentially mediated by a cumulative effect of MHC-II molecules-dependent
249 and independent mechanisms.
250 We next sought to determine whether the observed killing phenotype was orchestrated by $CD3^+$
251 T-cells. Similar to PBMCs, purified $CD3^+$ T-cells alone efficiently induced tumor cell killing in P3
252 organoids infected with Ad-CIITA (76,4%±21,9) or Ad-CIITA mutant (75,1%±29,4), suggesting a
253 primary T-cells involvement (**Fig. 4C vs 4B**). An additional effect from other immune cells cannot
254 be completely ruled out. To assess the specificity of Ad-CIITA induced T-cell killing, we performed
255 co-culture experiments with purified $CD4^+$ and $CD8^+$ T-cells, which rely on MHC-II and MHC-I
256 molecules, respectively. Interestingly, efficient tumor cell killing was maintained when GBM
257 organoids were co-cultured solely with either $CD4^+$ T-cells (Ad-CIITA: 75,6%±16,8) or $CD8^+$ T-cells
258 (Ad-CIITA: 67,5%±28,8) (**Fig. 4C**). Similar results were obtained with T16 and T188 organoids
259 (**Supplementary Fig. 4C**), reinforcing the involvement of a MHC-II independent mechanism in
260 GBM cell killing.
261 To further delineate the role of MHC-II molecules in the observed increased immunogenicity
262 mediated by Ad-CIITA and Ad-CIITA mutant for alloreative T-cells, we set up a co-culture system
263 with effector cells sharing a partial match at HLA alleles with the target GBM organoids.
264 Specifically, PBMCs were chosen to match the HLA typing of the donor GBM tumors at least at
265 one allele of each MHC class I (MHC-I) (*HLA-A*, *HLA-B*, *HLA-C*) and each MHC-II (*HLA-DRB1/3/4/5*,
266 *HLA-DQA1*, *HLA-DQB1*, *HLA-DPA1*, *HLA-DPB1*) locus. The matching degree varied depending on
267 the donor, as presented in **Table S3**. The Ad-CIITA-mediated killing phenotype was retained in the
268 P3 co-culture model (**Fig. 4D**) and confirmed in T16 tumors (**Supplementary Fig. 4D**). Although the

269 cytotoxic activity of HLA-matched PBMCs and isolated $CD3^+$ cells was reduced compared to
270 allogenic PBMC counterpart (**Fig. 4C vs Fig. 4D**), these data indicate that the main killing activity
271 observed could not be solely attributed to an alloreactive immune reaction linked to mismatching
272 MHC molecules.
273 In summary, our findings demonstrate that both Ad-CIITA and Ad-CIITA mutant enhance the
274 immunogenicity of GBM for allogenic T-cells, facilitating efficient tumor cell killing in the presence
275 of CD3+ T-cells. These data suggest that CIITA activates a T-cell mediated immune response that is
276 at least partially independent of MHC-II antigen presentation.

277 **Immune-mediated tumor cell killing of GBM organoids requires CIITA expression and cell-to-cell**
278 **contact with T-cells.**

279 To address the transgene specificity of the observed phenotype, we used an AdV carrying the *GFP*
280 transgene as a control. GFP expression was detected in P3 GBM organoids via live cell imaging at
281 24, 48, and 72 hours post-infection (**Fig. 5A**). Unlike Ad-CIITA, Ad-GFP did not lead to tumor cell
282 death upon co-culture with PBMCs (**Fig. 5B**). The same results were obtained in the T16 co-culture
283 model (**Supplementary Fig. 5A-B**), thus confirming the selectivity of the immune-mediated
284 phenotype toward CIITA.
285 Next, we aimed to determine whether the immune-mediated tumor killing required cell-to-cell
286 contact. We performed co-cultures using a two-layer transwell system, allowing for physical
287 separation of GBM organoids and immune cells, while maintaining the crosstalk via soluble
288 chemical mediators. In this setup, we observed the expected reduction in organoid growth due to
289 AdV infection, however organoid breakdown in the presence of Ad-CIITA and Ad-CIITA mutant
290 was completely abolished (**Fig. 5C**). This was replicated in T16 organoids (**Supplementary Fig. 5C**),
291 indicating that immune cells require direct cell-to-cell interaction with target GBM cells to
292 effectively induce tumor cell death.
293 To investigate whether AdV infection triggered other APC-like features in addition to MHC-II
294 molecules in infected GBM organoids, we conducted flow cytometry analysis of cell membrane
295 expression of costimulatory molecules CD80 and CD86, along with MHC-I. P3 GBM organoids
296 displayed positive MHC-I expression, which remained unaltered by AdV infection or CIITA
297 expression. Other surface co-stimulators were not expressed in GBM organoids either at baseline
298 or upon AdV /Adv-CIITA infection (**Supplementary Fig. 5D**).
299 We next aimed to assess different modes of contact-dependent T-cell-mediated cell killing.
300 Cytotoxic T-cells conventionally release lytic granules, such as perforin and granzymes, through
301 calcium-dependent exocytosis into the immunological synapse between cytotoxic T-cells and

302 target cells. However, degranulating T-cells did not appear to be involved in CIITA-mediated
303 killing, as evidenced by the absence of cell surface presentation of the degranulating marker
304 CD107a (**Fig. 5D**). Cell death can also be induced via activation of death receptor signaling in
305 target cells, including tumor necrosis factor alpha (TNF-α)/TNF-receptor (TNF-R) and Fas/Fas
306 ligand (FasL) (Barry and Bleackley 2002). We therefore selectively blocked these death pathways
307 via anti-human TNF-R and FasL monoclonal antibodies. Blocking either TNF- or Fas-mediated
308 signaling did not impact the ability of CIITA to induce the killing of GBM organoids (**Fig. 5E**), while
309 tumor cell killing induced by Actinomycin D and dimethyl sulfoxide (DMSO) was successfully
310 blocked by neutralizing TNF- and Fas-mediated signalling, respectively (**Supplementary Fig. 5E**).
311 As we did not detect classical T-cell activation mechanisms, we next investigated the differential
312 secretion of cytokines upon tumor cell killing mediated by Ad-CIITA (wild-type CIITA) (**Fig. 5F**).
313 Using conditioned media collected at 72 hours post co-culture, we detected increased secretion
314 of the extracellular matrix metalloproteinase inducer (EMMPRIN) and RANTES (Regulated upon
315 Activation, Normal T-cell Expressed, and Secreted) in Ad-CIITA co-culture medium. The secretion
316 of EMMPRIN, and consequently, the increased activity of metalloproteinases in degrading the
317 tumor extracellular matrix, might be linked with the observed CIITA-induced immune-mediated
318 organoid disruption preceeding tumor cell death. Moreover, compared to controls, the Ad-CIITA
319 co-culture medium exhibited decreased levels of IL-1alpha, IL-18, VEGF, and IL-6. This may
320 indicate a reduction of pro-tumorigenic, pro-angiogenic, and immunosuppressive potential of the
321 GBM tumor microenvironment upon Ad-CIITA infection. Whether these changes in cytokine levels
322 are functionally linked to tumor cell killing remains to be determined.

323 **DISCUSSION**

324 MHC-II molecules are the restricting elements of antigen presentation and $CD4^+$ T helper cell
325 activation. Their expression is usually confined to professional APCs, including dendritic cells, B
326 cells, macrophages, but they can be induced upon cytokine stimuli in other cell types, including
327 endothelial and epithelial cells (Drozina, Kohoutek et al. 2005). CIITA is the master regulator of
328 MHC-II expression, and this biological function can be exploited to stimulate adequate triggering
329 of the T helper arm of adaptive immunity against the tumor, a necessary requirement for effector
330 immune responses (Accolla, Ramia et al. 2019).
331 Given the need to develop new strategies against GBM tumors, we equipped a non-lytic AdV with
332 the wild-type *CIITA* transgene (Ad-CIITA). This proof-of-concept study employed a serotype 5
333 AdV, which could face reduced gene delivery efficiency due to pre-existing immunity to AdVs. For
334 *in vivo* application, various AdV vectors with genetic modifications could be developed to mitigate

335 immune responses and enhance gene delivery efficiency. At basal level, GBM tumor cells
336 generally lacked MHC-II expression, while other components of the MHC-II transcriptional
337 machinery were present. We show that Ad-CIITA infection of GBM cells resulted in robust MHC-II
338 expression at the surface of infected GBM cells.
339 Initially planned as a control vector, we generated a novel *CIITA* mutant harboring a point
340 mutation that encodes a full-length protein in which the glycine at position 1088 is replaced by an
341 arginine. This mutation resides within the carboxy-terminal region of CIITA. The replacement of
342 the non-polar, small amino acid glycine with arginine, a larger and positively charged amino acid,
343 may lead to alterations in the overall structure and electrostatic interactions within the protein,
344 impacting its folding, stability and binding properties (Molnár, Szakács and Tusnády 2016).
345 Structurally, a fully functional MHC-II transactivator consists of an amino-terminal acidic domain,
346 a proline/serine/threonine-rich region, a central GTP binding domain and a string of four leucine-
347 rich repeats (LRRs), which is essential for CIITA nuclear localization, enhanceosome assembly and
348 CIITA transactivator activity (Leon Machado and Steimle 2021). The positively charged mutation
349 presented in this study was found to reside in the fourth LRR, spanning from amino acid position
350 1073 to 1093. This novel mutation impeded the translocation of the CIITA master regulator to the
351 cell nucleus, thereby abrogating its role as a transcriptional coactivator. While a wild-type CIITA
352 protein typically exhibits a rather balanced distribution between the nucleus and cytoplasm
353 (roughly 50:50 ratio) (Leon Machado and Steimle 2021), the G1088A mutant protein was
354 effectively excluded from the nucleus. A previous study showed that the carboxy-terminal region
355 of CIITA is essential for its functionality as substitution of phenylalanine with serine at position
356 962 also abrogated MHC-II expression (Towey and Kelly 2002). Our novel point-mutated CIITA
357 variant may thus effectively serve to unravel MHC-II-dependent and -independent activities of
358 CIITA.
359 We here demonstrate that while Ad-CIITA infection has limited impact on tumor cell growth,
360 effective killing of infected GBM organoids is activated and maintained only in the presence of
361 immune cells. Our study reveals a new ability of CIITA to activate T-cells which is independent of
362 MHC-II molecules and antigen presentation. Firstly, we find that the CIITA mutant, unable to
363 translocate into the nucleus and therefore to induce MHC-II is still able to trigger a T-cell
364 mediated GBM tumor cell death. Secondly, in our model, CIITA wild type is also able to activate a
365 MHC-II independent immunity, as depletion of $CD4^+$ cells only partly impaired the ability of the
366 protein to activate immune cell death. A direct influence of the viral infection could be ruled out
367 since control empty and GFP-containing vectors had a significantly lesser effect on T-cell
368 activation or tumor cell death induction. Our findings indicate that the tumor killing phenotype
369 relies on direct cell-to-cell interaction between target GBM and immune cells. Interestingly, we

370 did not detect activation of canonical T-cell granule exocytosis or of known death signaling
371 pathways like Fas/FasL or TNF-α/TNF-R. The mechanism by which CIITA induces a MHC-II
372 independent immune-mediated tumor cell death remains to be characterized.
373 We show that the cytotoxicity induced by both Ad-CIITA and Ad-CIITA mutant in patient-derived
374 GBM cells was primarily mediated by $CD3^+$ T-cells, which is in line with *in vivo* results in mice of
375 *CIITA* transfection in the TS/A murine mammary adenocarcinoma model (Meazza, Comes et al.
376 2003, Frangione, Mortara et al. 2010) and GL261 glioma model (Celesti, Gatta et al. 2023).
377 Nevertheless, we cannot currently exclude the involvement of other immune components.
378 Further investigation should be directed in validating the anticancer role of cytoplasmic CIITA in
379 humanized GBM animal models, by examining whether T-cell-mediated immune recognition can
380 lead to tumor rejection or growth retardation following orthotopic injection of Ad-CIITA mutant-
381 infected GBM cells.

382 It has already been shown that CIITA not only governs the transcription of MHC-II genes but also
383 modulates the expression of other immune-related target genes, such as MHC-I, Plexin-A1, and
384 collagen type I α2, among others (Leon Machado and Steimle 2021). Our findings suggest that
385 CIITA may have additional roles in the cytoplasm, next to its well-established nuclear
386 transcriptional activation function. Previous research has described cytoplasmic effects of CIITA,
387 such as the L1035P CIITA mutant enhancing human immunodeficiency virion maturation through
388 Gag processing by the viral protease (Porter, Kelley et al. 2010).

389 T-cell activation and proliferation commonly require at least two key events: (i) T-cell receptor
390 (TCR) binding to a specific MHC-restricted antigen, and (ii) the interaction of costimulatory
391 molecules on the surface of T-cells and APCs. We have shown that the killing phenotype relies on
392 direct cell-to-cell interaction between the target tumor organoids and the immune cells and was
393 observed despite the absence of CD80 and CD86 costimulatory molecules, which is in line with
394 previous reports (Meazza, Comes et al. 2003, Mortara, Castellani et al. 2006, Frangione, Mortara
395 et al. 2010).
396 A protein cytokine array revealed increased secretion of EMMPRIN and RANTES along with a
397 decrease in various pro-inflammatory cytokines in Ad-CIITA co-culture medium. EMPPRIN is a
398 glycoprotein expressed and secreted by various cell types, including lymphocytes and tumor cells,
399 and is known to play a role in metalloproteinase induction, energy metabolism, T-cell activation,
400 co-stimulation, and proliferation (Kaushik, Yong et al. 2016). RANTES, also known as CCL5, is a
401 potent proinflammatory chemokine that acts either as a potent chemoattractant or as a mitogen-
402 like immune cell activator (Appay, Dunbar et al. 2000). RANTES-induced T-cell activation has
403 various effects, including lymphocyte proliferation or apoptotic cell death, as well as the release

404 of pro-inflammatory cytokines (Appay, Dunbar et al. 2000). Further studies are warranted to gain
405 a comprehensive understanding of the implications of soluble EMMPRIN and RANTES in the
406 observed T-cell-mediated killing phenotype.
407 In conclusion, our findings highlight the potential of viral delivery of the *CIITA* transgene in human
408 GBM as a promising immunotherapeutic approach for enhancing adaptive responses against
409 GBM. The observed T-cell-mediated cytotoxicity, partially independent of MHC-II antigen
410 presentation, opens up new avenues for further investigation into CIITA function beyond its
411 canonical nuclear transcriptional activation and MHC-II antigen presentation. Further elucidation
412 of the mechanism of T-cell-mediated tumor cell death is needed to understand the specific effects
413 induced by CIITA in the tumor cell cytoplasm. Additionally, it would be interesting to explore the
414 involvement of other immune cell subsets, such as natural killer cells and macrophages, in CIITA-
415 induced immune responses and to study potential immunosuppressive molecules induced by
416 CIITA treatment, as prolonged MHC-II molecules expression is commonly associated with
417 increased PD-1 expression (Chih, Sahm et al. 2021).

418 **MATHERIALS AND METHODS**

419 **Patient-derived preclinical models and cell culture.**

420 Human GBM patient tumor tissues were provided by the Department of Neurosurgery of the
421 Centre Hospitalier de Luxembourg, Luxembourg and the Neurosurgical Department of Haukeland
422 University Hospital, Bergen, Norway. Patient provided their informed consent, and the study was
423 accepted by the local ethical committees (the National Committee for Ethics in Research (CNER)
424 Luxembourg, under the protocol number 201201/06, and the Haukeland University Hospital,
425 under the protocol number 2009/117). PDOX models were generated and maintained by cycles of
426 short-term organoid cultures and orthotopic xenografting as previously described (Oudin, Baus et
427 al. 2021) (Golebiewska, Hau et al. 2020).
428 Patient-derived models expressing dsRed (P3dsRed and T16dsRed) were created from the original
429 PDOXs by stable transfection of a dsRed-expressing lentiviral vector (a three-vector system:
430 transfer vector pRRLsin-PPThCMV, helper plasmids pCMVdeltaR8.74, and VSV-G pMD.G.2) in GBM
431 organoids *ex vivo* as previously described (Niclou, Danzeisen et al. 2008). To perform *ex vivo*
432 experiments in GBM organoids, tumor cells were purified with use of previously published
433 protocol, which includes MACS-based purification of GBM cells from enzymatically-digested PDOX
434 tumor tissue and subsequent recreation of uniform organoids *ex vivo* (Oudin, Baus et al. 2021).
435 PDOX-derived organoids were cultured in Dulbecco's modified Eagle's medium (DMEM)
436 containing 4.5 g/L glucose w/o glutamine supplemented with 10% fetal bovine serum (FBS), 2 mM

437 UltraGlutamine, 0.4 mM nonessential amino acids (NEAAs) and 100 U/mL penicillin–streptomycin
438 ("Organoid medium").
439 Human GBM stem-like cell (GSC) lines, BG5, BG7, GG6 and GG16, and adherent GBM cell lines
440 U87 and U251 were kindly provided by Prof. Rolf Bjerkvig from University of Bergen. GSC lines
441 NCH421, NCH644 and NCH465 were kindly provide by Prof. Christel Herold-Mende from
442 University of Heidelberg. Human GSC lines P3NS and T16NS were generated from PDOX models as
443 previously described (Golebiewska, Hau et al. 2020). GSC lines were cultured as 3D spheres in
444 serum-free Neurobasal medium supplemented with 1X B-27™ Supplement, 2 mM UltraGlutamine,
445 0,1 U/mL heparin, 20 ng/mL bFGF, 20 ng/mL EGF and 100 U/mL penicillin–streptomycin ("NCS
446 medium"). Human embryonic kidney 293 T (293T) cells were obtained from ATCC. Murine GL261
447 glioma were kindly provided by Prof. Roberto Accolla from University of Insubria. All cell lines
448 were grown in DMEM high glucose, GlutaMAX™ supplemented with 10% FBS and 100 U/mL
449 penicillin–streptomycin ("DMEM medium"). All cells were maintained at 37°C in a 5% CO^2
450 atmosphere and 90% humidity and regularly tested for mycoplasma.

451 **HLA typing.**

452 Genomic DNA was extracted from GBM organoids with the commercially available DNeasy Blood
453 & Tissue Kit (Qiagen) according to the manufacturer's instructions. A total of 1200 ng was used for
454 ultrahigh resolution six-digits sequencing at 11 HLA loci (MHC-I *HLA-A*, *-B*, *-C*; MHC-II *HLA-*
455 *DRB1/3/4/5*, *-DQA1*, *-DQB1*, *-DPA1*, *-DPB1*) using the Illumina TruSight HLA v2 Sequencing panel
456 (**Table S3**).

457 **Gene expression analysis.**

458 The expression of MHC-II associated genes in GBM patient tumors and control normal brain tissue
459 was investigated with the GEPIA2 tool (Tang, Kang et al. 2019), which allows for exploration of
460 large-scale gene expression datasets from The Cancer Genome Atlas (TCGA) and the Genotype-
461 Tissue Expression (GTEx) projects. To examine gene expression in single cells isolated from GBM
462 patient tumors, we exploited the GBmap dataset (Ruiz-Moreno, Salas et al. 2022). The DotPlot
463 function in the Seurat package for R was applied to visualize gene expression changes in selected
464 cell populations. Gene expression in preclinical models was assessed with the Gene-Chip® Human
465 Gene 1.0ST Arrays (Affimetrix) as described previously (Golebiewska, Hau et al. 2020) or RNA-
466 sequencing (RNA-seq) on a bulk tissue. For bulk RNA-seq, total RNA was isolated from
467 cryopreserved PDOX tumor tissue using direct-zol RNA miniprep kit (Zymo Research). RNA quality
468 was checked with the HS RNA (15 nt) Kit (Agilent). mRNA-seq profiling was carried out with 50
469 million reads/sample, 2x150bp, using the Illumina Stranded mRNA prep kit on an Illumina

470 NovaSeq 6000 sequencer. RNA-seq quality control was performed using FastQC. Adaptors were
471 trimmed from raw sequencing reads using Cutadapt version 3.7 (Martin 2011), and the trimmed
472 reads were aligned to both the human reference genome GRCh38 and the mouse reference
473 genome GRCm39 by STAR 2.7.10b aligner (Dobin, Davis et al. 2013). Deconvolution of mouse and
474 human sequencing reads was performed with XenofilterR (Kluin, Kemper et al. 2018), which
475 separates mouse from human sequence reads. Uniquely human-mapped reads were ultimately
476 used to quantify gene expression using FeatureCounts (Liao, Smyth and Shi 2014). The R package
477 DGEobj.utils was used to normalize gene expression controlling for both library size and the gene
478 lengths, by converting raw counts to TPM (transcripts per million). Heatmap was generated using
479 the R package Pheatmap. All analyses were performed with R version 4.2.0.

480 **Peripheral blood lymphocytes.**

481 Allogeneic PBMCs were obtained from healthy human donors from the Red Cross of Luxembourg,
482 without controlling for HLA genotype. Allogeneic HLA-matched PBMCs were purchased from
483 Immunospot based on their HLA matching at MHC-I and MHC-II loci with the GBM organoids
484 (**Table S3**). The PBMC fraction was isolated from peripheral blood by density gradient
485 centrifugation and cryopreserved until later use. Cryopreserved human PBMCs were thawed at
486 37°C for 10-15 seconds in RPMI 1640 Medium, GlutaMAX™ supplemented with 9% FBS, 1%
487 human serum, 1 mM Sodium Pyruvate, 55 µM 2-Mercaptoethanol, 0,1 mM NEAA, 5 mM HEPES
488 and 100 U/mL penicillin-streptomycin ("T-cell medium"). After thawing, cells were incubated for
489 10 minutes with 25 U/mL benzonase (Sigma–Aldrich). Allogeneic HLA-matched PBMCs were
490 instead thawed, according to Immunospot's protocol.

491 To establish co-cultures involving specific T-cell populations, we first isolated human $CD3^+$ T-cells
492 from PBMCs using a $CD3^+$ T-cell negative isolation kit (Biolegend), according to the manufacturer's
493 instructions. Subsequently, we further separated $CD4^+$ and $CD8^+$ T-cell subsets from the
494 negatively-selected $CD3^+$ T-cells using the respective $CD4^+$ and $CD8^+$ T-cell negative isolation kits
495 (Miltenyi), according to the manufacturer's instructions. The purity of the isolated lymphocyte
496 fractions was evaluated using multi-color flow cytometry analysis. **Table S2** presents the
497 composition of PBMCs and the purity of the isolated sub-populations prior to co-culturing as
498 percentage of $CD45^+$ cells.

499 **AdV vectors.**

500 The plasmid pcFG3CIITA8 was originally created by J. Ting (Chin, Li and Ting 1997). The human
501 CIITA cDNA contained in pcFG3CIITA8 was first cloned into an intermediate pShuttle vector

502 (pShuttle-CIITA) and then homologous recombined into an AdV backbone, according to the Ad-
503 Easy-1 protocol (He, Zhou et al. 1998). The resulting Ad-CIITA vector encodes MHC-II
504 TransActivator isoform III (NP_000237.2, 1130 aa). AdVs containing a mutated version of CIITA
505 (Ad-CIITA mutant) and a CMV promoter without transgene (Ad-null) were used as controls. Sanger
506 sequencing revealed that Ad-CIITA mutant contains a mutation at amino acid position 1088
507 (glycine to arginine). This mutation was visualized using PyMOL molecular visualization tool. For
508 all vectors, the AdV backbone represents a first-generation replication-deficient (ΔE1-E3)
509 adenovirus serotype 5, and transgene expression is regulated via the CMV promoter.

510 **AdV production and titration.**

511 AdV plasmids were digested with PacI restriction enzyme to linearize the DNA and therefore
512 expose the two ITRs necessary for virus production. Once linearized, the AdV vector DNA was
513 transfected into adherent 293T-cells with Lipofectamine™ LTX Reagent with PLUS™ Reagent
514 (Thermo Fisher) according to the manufacturer's instructions. Virus was harvested at 70-80%
515 cytopathic effect (CPE), submitted to three rounds of freeze (liquid nitrogen)/thaw (37°C) cycles,
516 and then centrifuged at 2000 rpm for 10 minutes at RT. After two rounds of amplification in 293T-
517 cells, the AdV particles were harvested at 50% CPE and purified via a chromatography-based
518 system via an Adeno-X™ Maxi Purification Kit (Takara), following the manufacturer's instructions.
519 All recombinant AdVs were titrated at the same time using the Adeno-X Rapid Titer kit (Takara)
520 according to the manufacturer's protocol. Briefly, 293T-cells were infected with 10-fold serial
521 dilutions of the viral stock from 10^{-2} to 10^{-6} and, 48 hours post-infection, were fixed in ice-cold
522 methanol and stained with a primary antibody specific for the AdV hexon protein. Virus titer is
523 expressed as infectious units (IU)/mL.

524 **AdV infection.**

525 As a standard procedure, AdV infection was conducted on the same day as cell seeding. To
526 prevent potential inactivation of viral particles due to proteins of the fetal bovine serum, AdVs
527 were diluted in serum-free media. Non-infected cells were used as internal controls and treated
528 with virus-free serum-free media. The choice of medium depended on the target cells to be
529 infected. For murine (GL261) and human (U251) cell lines, seeding was performed in DMEM
530 medium, and virus infection was carried out in serum-free DMEM medium. In the case of GSC
531 lines (P3NS and T16NS), cell seeding and virus infection were both performed using NSC medium,
532 as this medium does not contain serum. Afterward, both non-infected and AdV-infected cells
533 were gently shaken every 15-20 minutes for an hour to facilitate virus adhesion to the host cell

534 membrane and subsequent entry. Subsequently, they were incubated at 37°C for a maximum of
535 six days post-infection. At day 6, cells were gently transferred in a bigger well and the medium
536 replenished.
537 As for the infection of primary GBM organoids, cryopreserved GBM single cells (P3, T16, and
538 T188), purified from PDOX tumor tissue *in vivo*, were thawed and seeded in 50 µL of organoid
539 medium in 96-well, Nunclon Sphera-Treated, U-Shaped-Bottom, ultra-low attachment microplates
540 (Thermo Fisher). Tumor cells were plated at a density of $2E10^4$ cells/well and then directly
541 infected with 50 µL of AdVs diluted in serum-free organoid medium. Non-infected GBM organoids
542 were instead treated with 50 µL of virus-free serum-free organoid medium. Cells were then gently
543 shacked every 15-20 minutes for an hour, centrifuged at 300 x g for 5 minutes and then incubated
544 at 37°C on an orbital shaker at 40-50 rpm for up to six days post-infection, depending on the read-
545 out.

546 **Assessment of virus cytotoxicity.**

547 To assess virus cytotoxicity, mouse cell lines (GL261) were infected at different AdV multiplicity of
548 infection (MOIs, infectious unit/cell, IU/cell): 0 (non-infected control), 1,56, 3,1, 6,2, 12,5, 25, 50
549 and 100. 2.5% DMSO (Sigma–Aldrich) was used as a positive control to induce cell death. Growth
550 of AdV-infected cells was assessed via xCELLigence Real-Time Cell Analyzer over a period of 166
551 hours post-infection.
552 To assess virus cytotoxicity, human GBM organoids (P3dsRed, T16dsRed and cytolight rapid red
553 dye-labeled T188 organoids) were infected at different AdV MOIs: 0 (non-infected control), 1, 5,
554 10, 25, 50 and 75. Growth of AdV-infected organoids was assessed via Incucyte S3 live cell imaging
555 system for at least seven days post-infection.

556 **AdV-infected GBM organoid - immune cell co-culture.**

557 Three days prior co-culture, cryopreserved GBM single cells (P3dsRed, T16dsRed, and cytolight
558 red rapid dye-labeled T188) were infected with AdV particles at the desired virus MOI in a final
559 volume of 100 µL organoid medium. AdV infection was performed as described in the "AdV
560 infection" section. The 96-well, Nunclon Sphera-Treated, U-Shaped-Bottom, ultra-low attachment
561 (Thermo Fisher) were continuously agitated for three days and centrifuged daily at 300 × g for 3
562 minutes. GBM organoid formation and red fluorescence were monitored daily via Incucyte S3 live
563 cell imaging system. On the day of the co-culture, cryopreserved human immune cells were
564 thawed, counted and resuspended at $2\text{-}3E10^6$ cells/mL in T-cell medium. For all the three GBM
565 models, we co-cultured the infected GBM organoids with three allogeneic healthy donors (CR014,

566 CR015, and CR017). Moreover, for P3 model, we co-cultured the infected GBM organoids with
567 three allogeneic HLA-matched donors (CTL573, CTL500, and CTL640). Co-cultures were either
568 performed with PBMCs, $CD3^+$, $CD4^+$, or $CD8^+$ T-cell fractions. Immune cells were diluted in 100 µL
569 of T-cell medium to reach different target:effector (T:E) ratios: 1:1, 1:5, 1:10, and added to the
570 GBM organoids, reaching a final volume of 200 µL. Co-cultures were performed for up to 3-4 days
571 in the Incucyte S3 live cell imaging system in the presence of 25 U/mL IL-2 (Miltenyi) and 5 µg/mL
572 anti-CD28 antibody (Biolegend). Depending on the read-out and the specific patient-derived
573 model, the co-culture was stopped at 1, 2, 3 or 4 days after co-culture. At the co-culture endpoint,
574 100ul of culture supernatant was collected from each experimental well and stored it at -20°C.
575 GBM organoids were dissociated for flow cytometry analysis.

576 **Incucyte S3 live cell imaging.**

577 The Incucyte S3 live cell imaging system was used to monitor red fluorescent protein-expressing
578 GBM organoids in real time, which can provide valuable information on tumor cell viability over
579 time. GBM organoids were imaged daily for the first 3 days post seeding and/or infection and,
580 after the addition of the immune cells, every 4 hours for a maximum of 96 hours after co-culture,
581 depending on the tumor model. GBM organoids were imaged with 4X magnification for phase
582 contrast, bright-field, and red channels. Data were then analyzed using Incucyte 2022A software.
583 In the case of P3dsRed and T16dsRed tumor models, wherein tumor cells exhibited stable
584 expression of the dsRed fluorescent protein, we quantified tumor cell viability by continuously
585 monitoring the total integrated red fluorescence intensity (RCU x μm^2/Image) over time. Dying
586 tumor cells lose dsRed, enabling effective tracking of cell death and achieving precise
587 quantification through monitoring changes in red fluorescence intensity. As for T188 tumor
588 model, we transiently labeled T188 single tumor cells with 0.3 µM of Incucyte® Cytolight Rapid
589 Red Dye (Sartorius) according to the manufacturer's instructions. As for Cytolight-stained GBM
590 organoids, the red fluorescent signal persisted post-cell death. To assess tumor cell viability, the
591 focus was on evaluating the structural integrity of the organoids by measuring the red total area
592 (μm^2/Image) over time. An increase in the red fluorescent area served as an indicator of GBM
593 organoid disruption.

594 **Immunohistochemistry and immunofluorescence on paraffin sections.**

595 AdV-infected and non-infected GBM organoids (300-450 µm in size) were carefully transferred
596 with wide-bore pipette tips from the 96-well, Nunclon Sphera-Treated, U-Shaped-Bottom, ultra-
597 low attachment (Thermo Fisher) into 15 mL Falcon tubes. They were gently washed with ice-cold
598 1X PBS and fixed in 4% paraformaldehyde for 20-30 minutes at RT. Fixation time depends on the

599 organoid size. Organoid sedimentation was preferred over centrifugation to preserve organoid
600 structure. Organoids were then gently washed, resuspended in 2.5% agar diluted in water and
601 transferred into Tissue-Tek cryomolds (Sakura) kept on ice for 5-10 min until agar solidification. If
602 present, bubbles were removed with a needle. With the help of forceps, agar blocks were then
603 moved to cassettes for automated paraffin embedding. Immunohistochemical and
604 immunofluorescence staining was performed following standard procedures with the antibodies
605 listed in **Table S4**.

606 **Two-layer transwell co-culture assay.**

607 AdV-infected GBM organoid – PBMC co-cultures were carried out as described in "AdV-infected
608 GBM organoid – immune cell co-culture" section using a two-layer transwell model to investigate
609 the cell contact dependency of immune cell-mediated tumor killing. Transwell-96 with 0.4 µm
610 pore polyester membrane inserts (StemCell Technologies) were used to physically separate the
611 AdV-infected and non-infected GBM organoids from the immune cells, which were plated on top
612 of the transwell inserts. Immune cell-mediated tumor killing was assessed in real time via the
613 Incucyte S3 live cell imaging system.

614 **Degranulation and T-cell activation assay.**

615 To assess the degranulation activity of the T lymphocytes in the co-culture, flow cytometry was
616 performed to measure the surface expression of the degranulation marker CD107a (**Table S4)**.
617 AdV-infected GBM organoid – $CD3^+$ T-cell co-cultures were carried out as described in the "AdV-
618 infected GBM organoid – immune cell co-culture" section. At 24 and 48 hours post co-culture,
619 with a T:E ratio of 1:10, the GBM organoid – $CD3^+$ T-cells were incubated with anti-CD107a
620 antibody for 1 hour at 37°C. As a positive control, freshly thawed $CD3^+$ T-cells were stimulated
621 with a combination of 50 ng/mL phorbol 12-myristate 13-acetate (PMA) (Enzo Life Sciences) and 1
622 µg/mL ionomycin (Enzo Life Sciences) and incubated with BV785-conjugated anti-CD107a
623 antibody for 1 hour at 37°C. Both co-culture samples and positive controls were then incubated
624 for 4 hours at 37°C with BD GolgiStop™ (dilution 1:1000), containing monensin, and BD GolgiPlug
625 (dilution 1:500), containing brefeldin A. These protein transport inhibitors block intracellular
626 protein transport processes, leading to the accumulation of cytokines in the Golgi complex. $CD3^+$
627 T-cells from five different wells (~1 million cells) were pooled together, fixed, and acquired using
628 the NovoCyte Quanteon Flow Cytometer, and the resulting data were analyzed using FlowJo
629 version 10 software.

630 **Neutralization assay.**

631 AdV-infected GBM organoid – PBMC co-cultures were carried out as described in the "AdV-
632 infected GBM organoid – immune cell co-culture" section. At 72 hours post-infection and prior to
633 the addition of immune cells, organoids were treated with increasing concentrations of anti-
634 human TNF-RI/TNFRSF1A (0.16 µg/mL, 0.08 µg/mL, 0.04 µg/mL, and 0.02 µg/mL) and anti-human
635 Fas Ligand/TNFSF6 (20 ng/mL, 10 ng/mL, 5 ng/mL, and 2.5 ng/mL) monoclonal antibodies (**Table**
636 **S4**). Immune cell-mediated tumor killing was assessed in real time via the Incucyte S3 live cell
637 imaging system.

638 **Measurement of cytokine secretion.**

639 At 72 hours post co-culture, conditioned media from GBM organoid – PBMC co-cultures were
640 collected, followed by centrifugation to remove particulates, and then stored at -20°C. To avoid
641 protein degradation, repeated freeze-thaw cycles were avoided. These co-culture supernatants
642 were subsequently screened using the Proteome Profiler Human XL Cytokine Array Kit (R&D),
643 capable of detecting 105 different cytokines simultaneously, following the manufacturer's
644 instructions. For each infection condition (Non-infected, Ad-null, Ad-CIITA), a total volume of 380
645 µL of co-culture supernatant was used per membrane of the cytokine array kit. Once the
646 complete protocol was executed, each membrane was simultaneously exposed to X-Ray films
647 with multiple exposure times (1, 5, and 10 minutes). The average signal (pixel density) per analyte
648 was quantified using Quick Spots software.

649 **Western blot.**

650 Total proteins from AdV-infected and non-infected mouse cell lines and human GSCs were
651 extracted in RIPA lysis buffer (Thermo Fisher) supplemented with protease and phosphatase
652 inhibitors (Thermo Fisher) for 45 minutes at 4°C and then quantified using a bicinchoninic acid
653 (BCA) protein assay. Heat-denatured protein samples were then separated on NuPage 4-12%
654 BisTris gels (Thermo Fisher) and blotted onto PVDF membranes. To prevent nonspecific antibody
655 binding, membranes were then blocked in 4% (wt/vol) skimmed milk in 1X Tris-Buffered Saline
656 with 0.1% Tween 20 (1X TBS-T) for 1 hour at room temperature (RT). Membranes were first
657 incubated with anti-CIITA and anti-HLA-DR primary antibodies diluted in blocking solution
658 overnight at 4°C and, after washing steps in 1X TBS-T, with horseradish peroxidase (HRP)-
659 conjugated secondary antibodies diluted in blocking solution for 1 hour at RT. Anti-GAPDH and
660 anti-LaminB1 primary antibodies were used as internal loading controls. A detailed list of the
661 antibodies and dilutions is available in **Table S4**. The chemiluminescent signal was revealed using
662 the Pierce™ ECL Western Blotting Substrate (Thermo Fisher) using the ImageQuant LAS4010
663 analyzer.

664 **Quantitative RT–PCR.**

665 Total RNA from AdV-infected and non-infected mouse cell lines and human GSCs was extracted
666 using the RNeasy Mini Kit (Qiagen) and reverse-transcribed to cDNA to measure CIITA and MHC-II
667 gene expression using Fast SYBR Green (Thermo Fisher) and QuantStudio 5 Real-Time PCR System.
668 It was run in biological triplicates, and the relative gene expression levels were calculated through
669 the ΔCT method by using *elongation factor 1 alpha (EF1α)* as a housekeeping gene. The primers
670 used were as follows: CIITA (Fw: TTATGCCAATATCGCGGAACTG, Rv:
671 CATCTGGTCCTATGTGCTTGAAA), HLA-DRα (Fw: AGTCCCTGTGCTAGGATTTTTCA, Rv:
672 ACATAAACTCGCCTGATTGGTC), EF1α (Fw: TTGTCGTCATTGGACACGTAG, Rv:
673 TGCCACCGCATTTATAGATCAG), and GAPDH (Fw: CTCCCACTCTTCCACCTTCG, Rv:
674 CCACCACCCTGTTGCTGTAG).

675 **Immunofluorescence.**

676 U251 cells were seeded at a density of $5E10^4$ cells/well in 8-well μ-slides (Ibidi). Cells were kept
677 overnight at 37°C and then either infected with AdVs or left uninfected. Three days post-infection,
678 cells were fixed with 4% PFA for 15 minutes at RT and, after washing steps in 1X PBS, blocked in
679 1X PBS with 0.5% Triton X-100 and 10% FBS for 1 hour at RT. Cells were then incubated with anti-
680 CIITA primary antibodies diluted in 1X PBS with 0.5% Triton X-100 overnight at 4°C. After three
681 washes in 1X PBS, the cells were incubated with fluorescently labeled secondary antibodies and
682 Hoechst dye diluted in 1X PBS with 0.01% BSA for 1 hour at RT. A detailed list of the antibodies
683 and dilutions used can be found in **Table S4**. Cells were then imaged with a Zeiss LSM 880
684 Confocal Laser Scanning Microscope and Zen Blue software.

685 **Flow cytometry.**

686 Single cells were stained with fluorochrome-conjugated antibodies diluted in ice-cold 1X
687 Phosphate-Buffered Saline (PBS) with 0,2% BSA ("FACS buffer") for 30 minutes at 4°C in the dark.
688 Alternatively, antibodies were diluted in ice-cold BD Horizon Brilliant Stain Buffer ("BV buffer") for
689 multicolor immunofluorescent staining using three or more brilliant violet antibodies. After wash,
690 cells were re-suspended in 100 μL of FACS buffer prior acquisition (1 million cells in 100 μL, we
691 scaled down accordingly for a smaller number of cells). Stained samples were then acquired with
692 NovoCyte Quanteon Flow Cytometer and the resulting data were analyzed using FlowJo version
693 10. A detailed list of all the antibodies and dilutions used can be found in **Table S4**.

694 **Statistical analysis.**

695 The experimental results were analyzed using GraphPad Prism 9 and reported as the mean ±
696 standard deviation (SD) or, for co-culture experiments, as mean ± standard error of mean (SEM).
697 One-way ANOVA was employed to compare multiple groups, while two-way ANOVA was used to
698 compare two or more factors simultaneously. All means were calculated based on a minimum of
699 three independent experiments. For tumor organoid-immune cell co-culture experiments, all
700 means were calculated based on a minimum of three immune cell donors, representing three
701 different biological replicates. A P value < 0.05 was used to determine statistical significance.

702 **ACKNOWLEDGEMENTS:** We are grateful for the use of the LIH PRECISION-PDX Brain Tumor Bank
703 (www.precision-pdx.lu), supported by the patients, the Neurosurgery Department of the Centre
704 Hospitalier de Luxembourg, the NORLUX Neuro-Oncology Laboratory and the Clinical and
705 Epidemiological Investigation Center of the LIH. We thank Prof. Roberto Accolla and Prof. Greta
706 Forlani for providing cell lines and critically reviewing the manuscript, Pilar M. Moreno-Sanchez
707 for technical assistance in the management of PDOXs, and the Luxembourg Croix Rouge and its
708 donors for generously providing healthy donor blood samples. We acknowledge the support from
709 LIH's core facilities (Animal facility, In vivo imaging facility, National Cytometry Platform, LUXGEN
710 sequencing platform).

711 **AUTHOR CONTRIBUTION:** Conceptualization (I. S., A.P. A.G., S.P.N., A.M.), methodology (I.S., E.K.,
712 A.P., M.R., A.C., A.G.), investigation (I.S., E.K., A.P., M.R., A.L., A.O., V.B., G.M.D.), formal analysis
713 (L.E., B.N., A.G.), supervision (A.P., A.G., S.P.N., A.M.) writing - original draft (I.S., A.G., S.P.N.,
714 A.M.), and writing – review & editing (all authors). The authors approved the final version of the
715 manuscript as submitted and agreed to be accountable for all the aspects of the work.

716 **CONFLICT OF INTEREST:** The authors have nothing to disclose.

717

718 **THE PAPER EXPLAINED:**

719 **Problem:** Glioblastoma (GBM) is a highly aggressive brain tumor with a poor prognosis. Current
720 immunotherapies for GBM have been largely unsuccessful due to the tumor's highly
721 immunosuppressive microenvironment. Consequently, there is an urgent need for new strategies
722 to boost immune responses against GBM.
723 **Results:** We successfully engineered and produced a non-lytic adenovirus (AdV) for the delivery to
724 cancer cells of CIITA, the master regulator of MHC-II antigen processing and presenting molecules.
725 The resulting AdV-induced MHC-II expression on GBM cell surfaces for at least six days post-

726 infection. Interestingly, infection with both an AdV carrying a wild-type nuclear CIITA and a
727 mutant cytoplasmic version of CIITA, but not with a GFP-armed AdV, resulted in substantial T-cell-
728 mediated tumor cell death. The latter was mediated via MHC-II-independent pathways, in
729 conjunction with MHC-II antigen presentation. Moreover, tumor cell death relied on direct
730 contact between GBM and immune cells, without involving canonical death pathways.
731 **Impact:** The study introduces a novel approach to combat the immunosuppressive GBM tumor
732 environment through AdV-mediated delivery of the *CIITA* transgene. This method shows promise
733 in enhancing T-cell-mediated immunity against GBM, providing a hopeful avenue for future GBM
734 treatment strategies. Additionally, it unveils an unexpected role of CIITA in triggering anti-tumor
735 immune responses that appears to be at least in part independent of MHC-II antigen
736 presentation.
737

738 **FUNDING INFORMATION:** We acknowledge the financial support by the Luxembourg Institute of
739 Health, FNRS-Télévie (GBModImm no. 7.8513.18, GBModImm2 no. 7651720F, ImmoGBM
740 7.8505.20, ImmoGBM2 7.6603.22) and the Luxembourg National Research Fund
741 (C20/BM/14646004/GLASSLUX, C21/BM/15739125/DIOMEDES).

742
743

744 **FIGURE LEGENDS**

745 **Figure 1. Correlation between CIITA and MHC-II expression in human GBM and associated**
746 **models. A**. Bulk RNA-seq gene expression of CIITA and selected MHC-II molecules in GBM patient
747 tumors (n=163) versus control normal brain (n=207). *p<0.01 (one-way ANOVA). **B.** Single cell
748 RNA-seq gene expression profiles in GBM patient tumors. Detected cells were classified into
749 tumor and non-neoplastic cells of the tumor microenvironment (top dot plot). Gene expression is
750 depicted for major cell types of the tumor microenvironment in GBM (bottom dot plot). The size
751 and color of each dot represent the percentage of cells within a class and the average expression
752 of a gene within a class, respectively. **C.** Heatmap representing bulk RNA-seq (human specific)
753 gene expression in GBM patient-derived orthotopic xenografts (PDOXs): selected MHC-II
754 molecules associated with enhanceosome, antigen processing, and presentation are shown.
755 *CXADR*, *ITGAV* and *ITGB5* are associated with AdV infection capacity. A lack of expression is
756 represented by the grey color; in every PDOX, the associated replicates are indicated by the
757 numbers. **D.** Flow cytometric analysis of MHC-II molecules at the cell membrane (anti-HLA-
758 DR/DP/DQ-FITC) in various GBM cell lines in control conditions (cells unstained or mock-
759 stimulated) and upon stimulation with IFN-γ.

760 **Figure 2. Characterization of Ad-CIITA in human glioblastoma stem-like cells (GSCs)**. **A**.
761 Schematic depicting the serotype 5 AdV (ΔE1-E3) vectors used in the study (see results for
762 details). **B-D**. Virus quality check in human GSC lines P3NS and T16NS infected at an MOI of 50.
763 CIITA and HLA-DRα expression at 72 hours post-infection. mRNA (**B**) and protein levels (**C**) of CIITA
764 and HLA-DRα were analyzed by quantitative RT–PCR and Western blot analysis, respectively. qRT–
765 PCR data were normalized to the amount of Ef1a, while Western blot data were normalized to the
766 amount of GAPDH. Mean ± SD. ***p<0.001 and ****p<0.0001 (one-way ANOVA). **D**. Surface
767 expression of MHC-II (anti-HLA-DR/DP/DQ-FITC) molecules was analyzed by flow cytometry at 72
768 hours and 6 days post-infection.

769 **Figure 3. Successful infection of human primary GBM organoids by Ad-CIITA vectors. A.** CIITA
770 and HLA-DRα expression levels in P3 GBM organoids infected with Ad-CIITA or control virus at
771 increasing MOIs (5, 10, 25, 50, 75) were analyzed by Western blot analysis at 72 hours post-
772 infection. **B-C.** P3 GBM organoids at MOI 50: Representative H&E (top) and anti-HLA-DRα
773 (bottom) staining at 72 hours post-infection (**B**). Flow cytometry analysis of cell surface expression
774 of MHC-II (anti-HLA-DR/DP/DQ-FITC) at 72 hours and 6 days post-infection (**C**). **D.** P3dsRed GBM
775 organoids infected with Ad-CIITA or control virus at increasing MOIs (5, 10, 25, 50, 75). Evaluation
776 of virus-mediated cytotoxicity as determined via the Incucyte S3 live cell imaging system. Graphs
777 represent tumor cell viability as total red integrated intensity (RCU x μm^2/Image) over a period of
778 186 hours post-infection. Results are expressed as mean ± SEM.

779 **Figure 4. Immune cell-mediated tumor cell killing in human primary GBM organoids induced by**
780 **Ad-CIITA and Ad-CIITA mutant A.** Schematic of the co-culture setup of Ad-infected GBM
781 organoids with immune cells. Red fluorescent GBM organoids were seeded and infected for 72
782 hours. Co-culture with effector cells (PBMCs, $CD3^+$, $CD4^+$, $CD8^+$) was performed in the presence of
783 IL-2 and anti-CD28 antibody for 3 days. Tumor cell viability was assessed using the IncucyteS3 live
784 cell imaging system. For the dsRed-expressing GBM organoids, viability was determined by
785 measuring the dsRed fluorescence levels, namely total red integrated intensity (RCU x μm^2/Image)
786 over time. **B-D.** Evaluation of viability of P3dsRed organoids infected at an MOI of 75. **B.** GBM

787 organoids alone (no co-culture) or in co-culture with PBMCs. **C.** GBM organoids in co-culture with
788 either purified $CD3^+$ T-cells, $CD4^+$ T-cells or $CD8^+$ T-cells. **D.** HLA-matched co-culture with either
789 PBMCs or purified $CD3^+$ T-cells.

790 Each co-culture panel includes: i) a graph displaying curves of tumor cell viability (measured as
791 total red integrated intensity [RCU x µm²/Image]) over a period of 134 hours after infection, ii) a
792 quantification of tumor cell viability at the co-culture endpoint (134 hours) at the tested T:E ratios
793 (indicated on the x-axis), and iii) representative phase contrast and red fluorescence images of
794 GBM organoids alone or in co-culture (T:E ratio of 1:10) with immune cells at the co-culture
795 endpoint (134 hours). Results are expressed as mean ± SEM. *p<0.05, **p<0.01, ***p<0.001, and
796 ****p<0.0001 (two-way ANOVA).

797 **Figure 5. Mechanisms of CIITA-mediated immune cell killing in human primary GBM organoids.**
798 **A-C.** P3dsRed organoids infected at a virus MOI of 75 and in co-culture with healthy donor PBMCs
799 at a 1:10 ratio. **A.** Representative live images of phase contrast and green fluorescence in Ad-GFP-
800 infected and non-infected organoids. Side quantification shows the total green integrated
801 intensity (GCU x µm²/Image) at 24, 48, and 72 hours post-infection compared to non-infected
802 control. Mean ± SD. ****p<0.0001 (two-way ANOVA). **B.** Immune-mediated tumor cell killing in
803 Ad-GFP- or Ad-CIITA-infected GBM organoids compared to non-infected control. Mean ± SEM.
804 ****p<0.0001 (one-way ANOVA). **C.** Immune-mediated tumor cell killing in two-layer transwell
805 co-culture. Graphs display curves of tumor cell viability (measured as total red integrated intensity
806 [RCU x µm²/Image] over a period of 134 hours post-infection. Side quantifications show tumor cell
807 viability at the co-culture endpoint (134 hours). Representative live images show phase contrast
808 and red fluorescence in GBM organoids at the co-culture endpoint (134 hours). Mean ± SEM.
809 **p<0.01 (one-way ANOVA). **D.** Surface expression of the degranulating marker CD107a in $CD3^+$ T-
810 cells at 24 hours post co-culture with infected organoids, as analyzed via flow cytometry assay.
811 The data are shown as overlay histograms (left panel) and graphs quantifying the mean
812 fluorescence intensity (MFI) (right panel) of CD107a in $CD4^+$ and $CD8^+$ T-cell populations. As
813 controls for T-cell activation, unstimulated $CD3^+$ T-cells and $CD3^+$ T-cells stimulated for 4 hours
814 with PMA and ionomycin were used as negative and positive controls, respectively. Mean ± SD.
815 **p<0.01 and ***p<0.001 (one-way ANOVA). **E.** Neutralization of death signaling pathways.
816 Organoids were treated with increasing concentrations of anti-human TNF-R (MAB225) (left
817 panel) and anti-human FasL (MAB126) (right panel) monoclonal antibodies and co-cultured with
818 healthy donor PBMCs. Mean ± SEM. **F.** Screening of conditioned media from GBM organoid-PBMC
819 co-cultures (T:E of 1:10) using a protein cytokine array (400 µL of cell supernatants, 10-minute
820 exposure). On the bottom left, heatmap of the most upregulated and downregulated proteins
821 detected via protein array based on mean pixel density. Each row represents a specific cytokine
822 with its array coordinates, while each column represents a co-culture condition. On the bottom
823 right, graphs show levels of secreted EMMPRIN and RANTES protein, expressed as mean pixel
824 density. Mean ± SD.
825

826 **SUPPLEMENTARY FIGURE LEGENDS**

827 **Supplementary Figure 1. MHC-II gene expression analysis in GBM patient tumors and human**
828 **preclinical models. A.** Heatmap representing gene expression levels of selected MHC-II molecules
829 associated with enhanceosome, antigen processing, presentation, and AdV viral infection capacity
830 in normal human brain, GBM patient tumors, patient-derived orthotopic xenografts (PDOXs), GSC
831 lines (NCH421k, NCH644), and classical glioma lines (U87, U251) grown *in vitro* or *in vivo* as
832 xenograft ('X'). A lack of expression is represented by the grey color. Human specific arrays were
833 applied for transcriptome analysis. **B.** Flow cytometric analysis of MHC-II cell membrane
834 expression (anti-HLA-DR/DP/DQ-FITC) in GBM cells in control conditions (cells unstained or mock-
835 stimulated) and upon stimulation with IFN-γ.

836 **Supplementary Figure 2. Characterization of viruses in adherent human (U251) and murine**
837 **(GL261) cell lines. A.** Sanger sequencing results of the *CIITA* mutant DNA show a guanine (g) to
838 adenine (a) genetic mutation in the *CIITA* gene that results in the substitution from a glycine (Gly)
839 to an arginine (Arg) at amino acid position 1088 of a full-length CIITA protein. **B.** Visual
840 representation of the amino acid string surrounding amino acid position 1088 (highlighted in
841 yellow) in wild-type (left panel) and mutated (right panel) CIITA protein. Molecular figures were
842 prepared via PyMOL. **C.** Representative confocal microscopy images of CIITA immunofluorescence
843 staining (Alexa Fluor 488) in human U251 cells at 72 hours post-infection. Nuclei were
844 counterstained in blue (Hoechst dye) (magnification 63X). The distribution of CIITA proteins
845 between the cytoplasm and nucleus was quantified by measuring the ratio of cytoplasmic to
846 nuclear fluorescence intensity. Mean ± SD. ****$p<0.0001$ (two-way ANOVA). **D-F.** Ad-CIITA
847 characterization in murine GL261 cells **D.** MHC-II (anti-IA-IE-PerCP) expression as a result of Ad-
848 CIITA infection at increasing virus MOIs (1.56, 3.1, 6.2, 12.5, 25, 50, 100, as analyzed by flow
849 cytometry. **E.** mRNA (left) and protein (right) levels of CIITA at 48 and 72 hours post-infection, as
850 analyzed by quantitative RT–PCR and by Western blot analysis, respectively. RT-PCR results were
851 normalized to the amount of GAPDH. Mean ± SD. ***$p<0.001$, ****$p<0.0001$ (two-way ANOVA).
852 Western Blot data were normalized to the amount of GAPDH. **F.** Kinetics of the expression of
853 MHC-II (anti-IA-IE-PerCP) molecules, as analyzed by flow cytometry.

854 **Supplementary Figure 3. Assessment of virus-mediated cytotoxicity in human primary GBM**
855 **organoids.** T16dsRed (top) and Cytolight Rapid Red Dye-labeled T188 (bottom) GBM organoids
856 infected with Ad-CIITA or control viruses at increasing MOIs (5, 10, 25, 50, 75). Evaluation of virus-
857 mediated cytotoxicity as determined via the Incucyte S3 live cell imaging system. Graphs
858 represent tumor cell viability as total red integrated intensity (RCU x μm^2/image) for T16dsRed
859 organoids, and red total area (μm^2/Image) for cytolight rapid red dye-labeled T188 organoids,
860 over a 186-hour post-infection period. Results are expressed as mean ± SEM.

861 **Supplementary Figure 4. Evaluation of immune cell-mediated tumor cell killing in human**
862 **primary GBM organoids. A.** Flow cytometry gating strategy to phenotype PBMCs and MACS-
863 purified isolated T-cell fractions. **B-C.** Evaluation of viability of T16dsRed (left panel) or of cytolight
864 rapid red dye-labeled T188 (right panel) organoids infected at an MOI of 25 or 75, respectively.
865 Deviations from the virus MOI are explicitly indicated on the graph. **B.** GBM organoids alone (no
866 co-culture) or in co-culture with PBMCs. In the case of cytolight rapid red dye-labeled T188
867 organoids, viability was assessed by measuring organoid integrity, namely the red total area

868 (µm^2/Image) over time. **C.** GBM organoids in co-culture with either purified CD3$^+$ T-cells, CD4$^+$ T-
869 cells or CD8$^+$ T-cells. **D.** Evaluation of viability of T16dsRed organoids infected at an MOI of 25 in
870 HLA-matched co-culture with either PBMCs or purified CD3$^+$ T-cells. T16dsRed co-culture panels
871 include: i) a graph displaying curves of tumor cell viability (measured as total red integrated
872 intensity [RCU x µm²/Image]) over a period of 170 hours after infection, ii) a quantification of
873 tumor cell viability at the co-culture endpoint (170 hours) at the tested T:E ratios (indicated on the
874 x-axis), and iii) representative Incucyte S3 phase contrast and red fluorescence images of GBM
875 organoids in co-culture (T:E ratio of 1:10) with immune cells at the co-culture endpoint. Mean ±
876 SEM. *p<0.05, **p<0.01, ***p<0.001, and ****p<0.0001 (two-way ANOVA). Cytolight-stained
877 T188 co-culture panels include: i) a quantification of tumor cell viability (measured as total red
878 area [µm²/Image]) at the co-culture endpoint (134 hours) at the tested T:E ratios (indicated on the
879 x-axis), and ii) representative Incucyte S3 phase contrast and red fluorescence images of GBM
880 organoids in co-culture (T:E ratio of 1:10) with immune cells at the co-culture endpoint. Mean ±
881 SEM. *p<0.05, **p<0.01, ***p<0.001, and ****p<0.0001 (two-way ANOVA).

882 **Supplementary Figure 5. Mechanisms of CIITA-mediated immune cell killing in human primary**
883 **GBM organoids. A-C.** T16dsRed organoids infected at a virus MOI of 25 and in co-culture with
884 healthy donor PBMCs at a 1:10 ratio. **A.** Representative Incucyte S3 images show phase contrast
885 and green fluorescence in Ad-GFP-infected and non-infected organoids. Side quantification shows
886 the total green integrated intensity (GCU x µm²/Image) at 24, 48, and 72 hours post-infection
887 compared to non-infected control. Mean ± SD. ****p<0.0001 (two-way ANOVA). **B.** Immune-
888 mediated tumor cell killing in Ad-GFP- or Ad-CIITA-infected GBM organoids compared to non-
889 infected control. Mean ± SEM. *p<0.05, **p<0.01 (one-way ANOVA). **C.** Immune-mediated tumor
890 cell killing in two-layer transwell co-culture. Graphs display curves of tumor cell viability
891 (measured as total red integrated intensity [RCU x µm²/Image] over a period of 170 hours post-
892 infection. Side quantifications show tumor cell viability at the co-culture endpoint (170 hours).
893 Representative Incucyte S3 images show phase contrast and red fluorescence in GBM organoids
894 at the co-culture endpoint (170 hours). Mean ± SEM. **D.** Flow cytometry analysis of cell surface
895 expression of MHC-I (anti-HLA-A/B/C-BV510), CD80 (anti-CD80-PE), CD86 (anti-CD86-BV421) as
896 analyzed by flow cytometry. **E.** Positive controls of death signaling pathway neutralization.
897 P3dsRed organoids were treated with (left) actinomycin D (1 µg/mL) and increasing
898 concentrations of anti-human TNF-R (MAB225) or with (right) 2.5% DMSO and anti-human FasL
899 (MAB126). Mean ± SEM.

900
901

902 **REFERENCES**

903 Accolla, R. S., E. Ramia, A. Tedeschi and G. Forlani (2019). "CIITA-Driven MHC Class II Expressing Tumor Cells
904 as Antigen Presenting Cell Performers: Toward the Construction of an Optimal Anti-tumor Vaccine." Front
905 Immunol **10**: 1806.

906 Agosti, E., M. Zeppieri, L. De Maria, C. Tedeschi, M. M. Fontanella, P. P. Panciani and T. Ius (2023).
907 "Glioblastoma Immunotherapy: A Systematic Review of the Present Strategies and Prospects for
908 Advancements." Int J Mol Sci **24**(20).

909 Appay, V., P. R. Dunbar, V. Cerundolo, A. McMichael, L. Czaplewski and S. Rowland-Jones (2000). "RANTES
910 activates antigen-specific cytotoxic T lymphocytes in a mitogen-like manner through cell surface
911 aggregation." International Immunology **12**(8): 1173-1182.

912 Banerjee, K., F. J. Nunez, S. Haase, B. L. McClellan, S. M. Faisal, S. V. Carney, J. Yu, M. S. Alghamri, A. S. Asad,
913 A. J. N. Candia, M. L. Varela, M. Candolfi, P. R. Lowenstein and M. G. Castro (2021). "Current Approaches for
914 Glioma Gene Therapy and Virotherapy." Front Mol Neurosci **14**: 621831.

915 Barry, M. and R. C. Bleackley (2002). "Cytotoxic T lymphocytes: all roads lead to death." Nat Rev Immunol
916 **2**(6): 401-409.

917 Bou Nasser Eddine, F., G. Forlani, L. Lombardo, A. Tedeschi, G. Tosi and R. S. Accolla (2017). "CIITA-driven
918 MHC class II expressing tumor cells can efficiently prime naive CD4(+) TH cells in vivo and vaccinate the host
919 against parental MHC-II-negative tumor cells." Oncoimmunology **6**(1): e1261777.

920 Bulcha, J. T., Y. Wang, H. Ma, P. W. L. Tai and G. Gao (2021). "Viral vector platforms within the gene therapy
921 landscape." Signal Transduct Target Ther **6**(1): 53.

922 Burster, T., F. Gärtner, C. Bulach, A. Zhanapiya, A. Gihring and U. Knippschild (2021). "Regulation of MHC I
923 Molecules in Glioblastoma Cells and the Sensitizing of NK Cells." Pharmaceuticals (Basel) **14**(3).

924 Celesti, F., A. Gatta, M. Shallak, A. M. Chiaravalli, M. Cerati, F. Sessa, R. S. Accolla and G. Forlani (2023).
925 "Protective anti-tumor vaccination against glioblastoma expressing the MHC class II transactivator CIITA."
926 Front Immunol **14**: 1133177.

927 Chih, Y., K. Sahm, A. Sadik, T. Bunse, N. Trautwein, S. Pusch, S. Stevanovic, C. Opitz, A. Deimling, W. Wick, F.
928 Sahm, L. Bunse and M. Platten (2021). "KS01.3.A Tumoral MHC class II expression in gliomas drives T cell
929 exhaustion." Neuro-Oncology **23**(Supplement_2): ii3-ii3.

930 Chin, K.-C., G. G.-X. Li and J. P.-Y. Ting (1997). "Importance of acidic, proline/serine/threonine-rich, and
931 GTPbinding regions in the major histocompatibility complex class II transactivator: Generation
932 of transdominant-negative mutants." Proceedings of the National Academy of Sciences **94**(6): 2501-2506.

933 Cloughesy, T. F., A. Brenner, J. F. de Groot, N. A. Butowski, L. Zach, J. L. Campian, B. M. Ellingson, L. S.
934 Freedman, Y. C. Cohen, N. Lowenton-Spier, T. Rachmilewitz Minei, S. Fain Shmueli and P. Y. Wen (2020). "A
935 randomized controlled phase III study of VB-111 combined with bevacizumab vs bevacizumab monotherapy
936 in patients with recurrent glioblastoma (GLOBE)." Neuro Oncol **22**(5): 705-717.

937 Cloughesy, T. F., K. Petrecca, T. Walbert, N. Butowski, M. Salacz, J. Perry, D. Damek, D. Bota, C. Bettegowda,
938 J.-J. Zhu, F. Iwamoto, D. Placantonakis, L. Kim, B. Elder, G. Kaptain, D. Cachia, Y. Moshel, S. Brem, D. Piccioni,
939 J. Landolfi, C. C. Chen, H. Gruber, A. R. Rao, D. Hogan, W. Accomando, D. Ostertag, T. T. Montellano, T.
940 Kheoh, F. Kabbinavar and M. A. Vogelbaum (2020). "Effect of Vocimagene Amiretrorepvec in Combination
941 With Flucytosine vs Standard of Care on Survival Following Tumor Resection in Patients With Recurrent
942 High-Grade Glioma: A Randomized Clinical Trial." JAMA Oncology **6**(12): 1939-1946.

943 Dobin, A., C. A. Davis, F. Schlesinger, J. Drenkow, C. Zaleski, S. Jha, P. Batut, M. Chaisson and T. R. Gingeras
944 (2013). "STAR: ultrafast universal RNA-seq aligner." Bioinformatics **29**(1): 15-21.

945 Drozina, G., J. Kohoutek, N. Jabrane-Ferrat and B. M. Peterlin (2005). "Expression of MHC II genes." Curr Top
946 Microbiol Immunol **290**: 147-170.

947 Forlani, G., M. Shallak, A. Gatta, A. K. B. Shaik and R. S. Accolla (2023). "The NLR member CIITA: Master
948 controller of adaptive and intrinsic immunity and unexpected tool in cancer immunotherapy." Biomed J
949 **46**(5): 100631.

950 Frangione, V., L. Mortara, P. Castellani, A. De Lerma Barbaro and R. S. Accolla (2010). "CIITA-driven MHC-II
951 positive tumor cells: preventive vaccines and superior generators of antitumor CD4+ T lymphocytes for
952 immunotherapy." Int J Cancer **127**(7): 1614-1624.

953 Golebiewska, A., A.-C. Hau, A. Oudin, D. Stieber, Y. A. Yabo, V. Baus, V. Barthelemy, E. Klein, S. Bougnaud, O.
954 Keunen, M. Wantz, A. Michelucci, V. Neirinckx, A. Muller, T. Kaoma, P. V. Nazarov, F. Azuaje, A. De Falco, B.
955 Flies, L. Richart, S. Poovathingal, T. Arns, K. Grzyb, A. Mock, C. Herold-Mende, A. Steino, D. Brown, P. May,
956 H. Miletic, T. M. Malta, H. Noushmehr, Y.-J. Kwon, W. Jahn, B. Klink, G. Tanner, L. F. Stead, M. Mittelbronn,
957 A. Skupin, F. Hertel, R. Bjerkvig and S. P. Niclou (2020). "Patient-derived organoids and orthotopic
958 xenografts of primary and recurrent gliomas represent relevant patient avatars for precision oncology."
959 Acta Neuropathologica **140**(6): 919-949.

960 He, T.-C., S. Zhou, L. T. da Costa, J. Yu, K. W. Kinzler and B. Vogelstein (1998). "A simplified system for
961 generating recombinant adenoviruses." Proceedings of the National Academy of Sciences **95**(5): 2509-2514.

962 Hillman, G. G., N. L. Kallinteris, J. Li, Y. Wang, X. Lu, Y. Li, S. Wu, J. L. Wright, P. Slos, J. V. Gulfo, R. E.
963 Humphreys and M. Xu (2003). "Generating MHC Class II+/Ii- phenotype after adenoviral delivery of both an
964 expressible gene for MHC Class II inducer and an antisense Ii-RNA construct in tumor cells." Gene Ther
965 **10**(17): 1512-1518.

966 Immonen, A., M. Vapalahti, K. Tyynelä, H. Hurskainen, A. Sandmair, R. Vanninen, G. Langford, N. Murray
967 and S. Ylä-Herttuala (2004). "AdvHSV-tk gene therapy with intravenous ganciclovir improves survival in
968 human malignant glioma: a randomised, controlled study." Mol Ther **10**(5): 967-972.

969 Kaushik, D. K., H. Y. Yong, J. N. Hahn, C. Silva, S. Casha, R. J. Hurlbert, F. H. Jacques, R. Lisak, O. Khan, C.
970 Ionete, C. Larochelle, A. Prat, A. Bar-Or and V. W. Yong (2016). "Evaluating Soluble EMMPRIN as a Marker of
971 Disease Activity in Multiple Sclerosis: Studies of Serum and Cerebrospinal Fluid." PLoS One **11**(10):
972 e0163802.

973 Kluin, R. J. C., K. Kemper, T. Kuilman, J. R. de Ruiter, V. Iyer, J. V. Forment, P. Cornelissen-Steijger, I. de Rink,
974 P. Ter Brugge, J. Y. Song, S. Klarenbeek, U. McDermott, J. Jonkers, A. Velds, D. J. Adams, D. S. Peeper and O.
975 Krijgsman (2018). "XenofilteR: computational deconvolution of mouse and human reads in tumor xenograft
976 sequence data." BMC Bioinformatics **19**(1): 366.

977 Leon Machado, J. A. and V. Steimle (2021). "The MHC Class II Transactivator CIITA: Not (Quite) the Odd-
978 One-Out Anymore among NLR Proteins." Int J Mol Sci **22**(3).

979 Liao, Y., G. K. Smyth and W. Shi (2014). "featureCounts: an efficient general purpose program for assigning
980 sequence reads to genomic features." Bioinformatics **30**(7): 923-930.

981 Liau, L. M., K. Ashkan, S. Brem, J. L. Campian, J. E. Trusheim, F. M. Iwamoto, D. D. Tran, G. Ansstas, C. S.
982 Cobbs, J. A. Heth, M. E. Salacz, S. D'Andre, R. D. Aiken, Y. A. Moshel, J. Y. Nam, C. P. Pillainayagam, S. A.
983 Wagner, K. A. Walter, R. Chaudhary, S. A. Goldlust, I. Y. Lee, D. A. Bota, H. Elinzano, J. Grewal, K. Lillehei, T.
984 Mikkelsen, T. Walbert, S. Abram, A. J. Brenner, M. G. Ewend, S. Khagi, D. S. Lovick, J. Portnow, L. Kim, W. G.
985 Loudon, N. L. Martinez, R. C. Thompson, D. E. Avigan, K. L. Fink, F. J. Geoffroy, P. Giglio, O. Gligich, D. Krex, S.
986 M. Lindhorst, J. Lutzky, H. J. Meisel, M. Nadji-Ohl, L. Sanchin, A. Sloan, L. P. Taylor, J. K. Wu, E. M. Dunbar, A.
987 B. Etame, S. Kesari, D. Mathieu, D. E. Piccioni, D. S. Baskin, M. Lacroix, S. A. May, P. Z. New, T. J. Pluard, S. A.
988 Toms, V. Tse, S. Peak, J. L. Villano, J. D. Battiste, P. J. Mulholland, M. L. Pearlman, K. Petrecca, M. Schulder,
989 R. M. Prins, A. L. Boynton and M. L. Bosch (2023). "Association of Autologous Tumor Lysate-Loaded

990 Dendritic Cell Vaccination With Extension of Survival Among Patients With Newly Diagnosed and Recurrent
991 Glioblastoma: A Phase 3 Prospective Externally Controlled Cohort Trial." JAMA Oncol **9**(1): 112-121.

992 Lim, M., M. Weller, A. Idbaih, J. Steinbach, G. Finocchiaro, R. R. Raval, G. Ansstas, J. Baehring, J. W. Taylor, J.
993 Honnorat, K. Petrecca, F. De Vos, A. Wick, A. Sumrall, S. Sahebjam, I. K. Mellinghoff, M. Kinoshita, M.
994 Roberts, R. Slepetis, D. Warad, D. Leung, M. Lee, D. A. Reardon and A. Omuro (2022). "Phase III trial of
995 chemoradiotherapy with temozolomide plus nivolumab or placebo for newly diagnosed glioblastoma with
996 methylated MGMT promoter." Neuro Oncol **24**(11): 1935-1949.

997 Martin, M. (2011). "CUTADAPT removes adapter sequences from high-throughput sequencing reads."
998 EMBnet.journal **17**.

999 Meazza, R., A. Comes, A. M. Orengo, S. Ferrini and R. S. Accolla (2003). "Tumor rejection by gene transfer of
1000 the MHC class II transactivator in murine mammary adenocarcinoma cells." Eur J Immunol **33**(5): 1183-
1001 1192.

1002 Molnár, J., G. Szakács and G. E. Tusnády (2016). "Characterization of Disease-Associated Mutations in
1003 Human Transmembrane Proteins." PLoS One **11**(3): e0151760.

1004 Mortara, L., P. Castellani, R. Meazza, G. Tosi, A. De Lerma Barbaro, F. A. Procopio, A. Comes, L. Zardi, S.
1005 Ferrini and R. S. Accolla (2006). "CIITA-induced MHC class II expression in mammary adenocarcinoma leads
1006 to a Th1 polarization of the tumor microenvironment, tumor rejection, and specific antitumor memory."
1007 Clin Cancer Res **12**(11 Pt 1): 3435-3443.

1008 Narita, Y., Y. Arakawa, F. Yamasaki, R. Nishikawa, T. Aoki, M. Kanamori, M. Nagane, T. Kumabe, Y. Hirose, T.
1009 Ichikawa, H. Kobayashi, T. Fujimaki, H. Goto, H. Takeshima, T. Ueba, H. Abe, T. Tamiya, Y. Sonoda, A.
1010 Natsume, T. Kakuma, Y. Sugita, N. Komatsu, A. Yamada, T. Sasada, S. Matsueda, S. Shichijo, K. Itoh and M.
1011 Terasaki (2019). "A randomized, double-blind, phase III trial of personalized peptide vaccination for
1012 recurrent glioblastoma." Neuro Oncol **21**(3): 348-359.

1013 Nemerow, G. R. and P. L. Stewart (1999). "Role of alpha(v) integrins in adenovirus cell entry and gene
1014 delivery." Microbiol Mol Biol Rev **63**(3): 725-734.

1015 Niclou, S. P., C. Danzeisen, H. P. Eikesdal, H. Wiig, N. H. C. Brons, A. M. F. Poli, A. Svendsen, A. Torsvik, P. Ø.
1016 Enger, J. A. Terzis and R. Bjerkvig (2008). "A novel eGFP-expressing immunodeficient mouse model to study
1017 tumor-host interactions." The FASEB Journal **22**(9): 3120-3128.

1018 Omuro, A., A. A. Brandes, A. F. Carpentier, A. Idbaih, D. A. Reardon, T. Cloughesy, A. Sumrall, J. Baehring, M.
1019 van den Bent, O. Bähr, G. Lombardi, P. Mulholland, G. Tabatabai, U. Lassen, J. M. Sepulveda, M. Khasraw, E.
1020 Vauleon, Y. Muragaki, A. M. Di Giacomo, N. Butowski, P. Roth, X. Qian, A. Z. Fu, Y. Liu, V. Potter, A. G.
1021 Chalamandaris, K. Tatsuoka, M. Lim and M. Weller (2023). "Radiotherapy combined with nivolumab or
1022 temozolomide for newly diagnosed glioblastoma with unmethylated MGMT promoter: An international
1023 randomized phase III trial." Neuro Oncol **25**(1): 123-134.

1024 Ostrom, Q. T., G. Cioffi, K. Waite, C. Kruchko and J. S. Barnholtz-Sloan (2021). "CBTRUS Statistical Report:
1025 Primary Brain and Other Central Nervous System Tumors Diagnosed in the United States in 2014-2018."
1026 Neuro Oncol **23**(12 Suppl 2): iii1-iii105.

1027 Oudin, A., V. Baus, V. Barthelemy, C. Fabian, E. Klein, M. Dieterle, M. Wantz, A. C. Hau, C. Dording, A.
1028 Bernard, A. Michelucci, Y. A. Yabo, G. Kanli, O. Keunen, R. Bjerkvig, S. P. Niclou and A. Golebiewska (2021).
1029 "Protocol for derivation of organoids and patient-derived orthotopic xenografts from glioma patient
1030 tumors." STAR Protoc **2**(2): 100534.

1031 Palma, M. L., P. Duangkhae, B. Douradinha, I. F. T. Viana, P. O. Rigato, R. Dhalia, R. B. Mailliard, S. M.
1032 Barratt-Boyes, E. J. M. Nascimento, T. M. Oshiro, A. J. da Silva Duarte and E. T. A. Marques (2017).
1033 "Development of potent class II transactivator gene delivery systems capable of inducing de novo MHC II
1034 expression in human cells, in vitro and ex vivo." Gene Ther **24**(6): 342-352.

1035 Pires-Afonso, Y., S. P. Niclou and A. Michelucci (2020). "Revealing and Harnessing Tumour-Associated
1036 Microglia/Macrophage Heterogeneity in Glioblastoma." Int J Mol Sci **21**(3).

1037 Porter, K. A., L. N. Kelley, A. George, J. A. Harton and K. M. Duus (2010). "Class II Transactivator (CIITA)
1038 Enhances Cytoplasmic Processing of HIV-1 Pr55Gag." PLOS ONE **5**(6): e11304.

1039 Quail, D. F. and J. A. Joyce (2017). "The Microenvironmental Landscape of Brain Tumors." Cancer Cell **31**(3):
1040 326-341.

1041 Rainov, N. G. (2000). "A phase III clinical evaluation of herpes simplex virus type 1 thymidine kinase and
1042 ganciclovir gene therapy as an adjuvant to surgical resection and radiation in adults with previously
1043 untreated glioblastoma multiforme." Hum Gene Ther **11**(17): 2389-2401.

1044 Reardon, D. A., A. A. Brandes, A. Omuro, P. Mulholland, M. Lim, A. Wick, J. Baehring, M. S. Ahluwalia, P.
1045 Roth, O. Bahr, S. Phuphanich, J. M. Sepulveda, P. De Souza, S. Sahebjam, M. Carleton, K. Tatsuoka, C. Taitt,
1046 R. Zwirtes, J. Sampson and M. Weller (2020). "Effect of Nivolumab vs Bevacizumab in Patients With
1047 Recurrent Glioblastoma: The CheckMate 143 Phase 3 Randomized Clinical Trial." JAMA Oncol **6**(7): 1003-
1048 1010.

1049 Ruiz-Moreno, C., S. M. Salas, E. Samuelsson, S. Brandner, M. E. G. Kranendonk, M. Nilsson and H. G.
1050 Stunnenberg (2022). "Harmonized single-cell landscape, intercellular crosstalk and tumor architecture of
1051 glioblastoma." bioRxiv: 2022.2008.2027.505439.

1052 Sartoris, S., M. T. Valle, A. L. Barbaro, G. Tosi, T. Cestari, A. D'Agostino, A. M. Megiovanni, F. Manca and R. S.
1053 Accolla (1998). "HLA class II expression in uninducible hepatocarcinoma cells after transfection of AIR-1
1054 gene product CIITA: acquisition of antigen processing and presentation capacity." J Immunol **161**(2): 814-
1055 820.

1056 Tang, Z., B. Kang, C. Li, T. Chen and Z. Zhang (2019). "GEPIA2: an enhanced web server for large-scale
1057 expression profiling and interactive analysis." Nucleic Acids Research **47**(W1): W556-W560.

1058 Thompson, J. A., S. K. Dissanayake, B. R. Ksander, K. L. Knutson, M. L. Disis and S. Ostrand-Rosenberg (2006).
1059 "Tumor cells transduced with the MHC class II Transactivator and CD80 activate tumor-specific CD4+ T cells
1060 whether or not they are silenced for invariant chain." Cancer Res **66**(2): 1147-1154.

1061 Towey, M. and A. P. Kelly (2002). "Nuclear localisation of CIITA is controlled by a carboxy terminal leucine-
1062 rich repeat region." Molecular Immunology **38**(8): 627-634.

1063 Weller, M., N. Butowski, D. D. Tran, L. D. Recht, M. Lim, H. Hirte, L. Ashby, L. Mechtler, S. A. Goldlust, F.
1064 Iwamoto, J. Drappatz, D. M. O'Rourke, M. Wong, M. G. Hamilton, G. Finocchiaro, J. Perry, W. Wick, J. Green,
1065 Y. He, C. D. Turner, M. J. Yellin, T. Keler, T. A. Davis, R. Stupp and J. H. Sampson (2017). "Rindopepimut with
1066 temozolomide for patients with newly diagnosed, EGFRvIII-expressing glioblastoma (ACT IV): a randomised,
1067 double-blind, international phase 3 trial." Lancet Oncol **18**(10): 1373-1385.

1068 Woroniecka, K., P. Chongsathidkiet, K. Rhodin, H. Kemeny, C. Dechant, S. H. Farber, A. A. Elsamadicy, X. Cui,
1069 S. Koyama, C. Jackson, L. J. Hansen, T. M. Johanns, L. Sanchez-Perez, V. Chandramohan, Y. A. Yu, D. D.
1070 Bigner, A. Giles, P. Healy, G. Dranoff, K. J. Weinhold, G. P. Dunn and P. E. Fecci (2018). "T-Cell Exhaustion
1071 Signatures Vary with Tumor Type and Are Severe in Glioblastoma." Clin Cancer Res **24**(17): 4175-4186.

1072 Zheng, C., C. M. Goldsmith, B. C. O'Connell and B. J. Baum (2000). "Adenoviral Vector Cytotoxicity Depends
1073 in Part on the Transgene Encoded." Biochemical and Biophysical Research Communications **274**(3): 767-
1074 771.

1075 Zhou, G., R. Lieshout, G. S. van Tienderen, V. de Ruiter, M. E. van Royen, P. P. C. Boor, L. Magré, J. Desai, K.
1076 Köten, Y. Y. Kan, Z. Ge, L. Campos Carrascosa, C. Geuijen, D. Sprengers, L. J. W. van der Laan, M. M. A.
1077 Verstegen and J. Kwekkeboom (2022). "Modelling immune cytotoxicity for cholangiocarcinoma with
1078 tumour-derived organoids and effector T cells." British Journal of Cancer **127**(4): 649-660.

1079

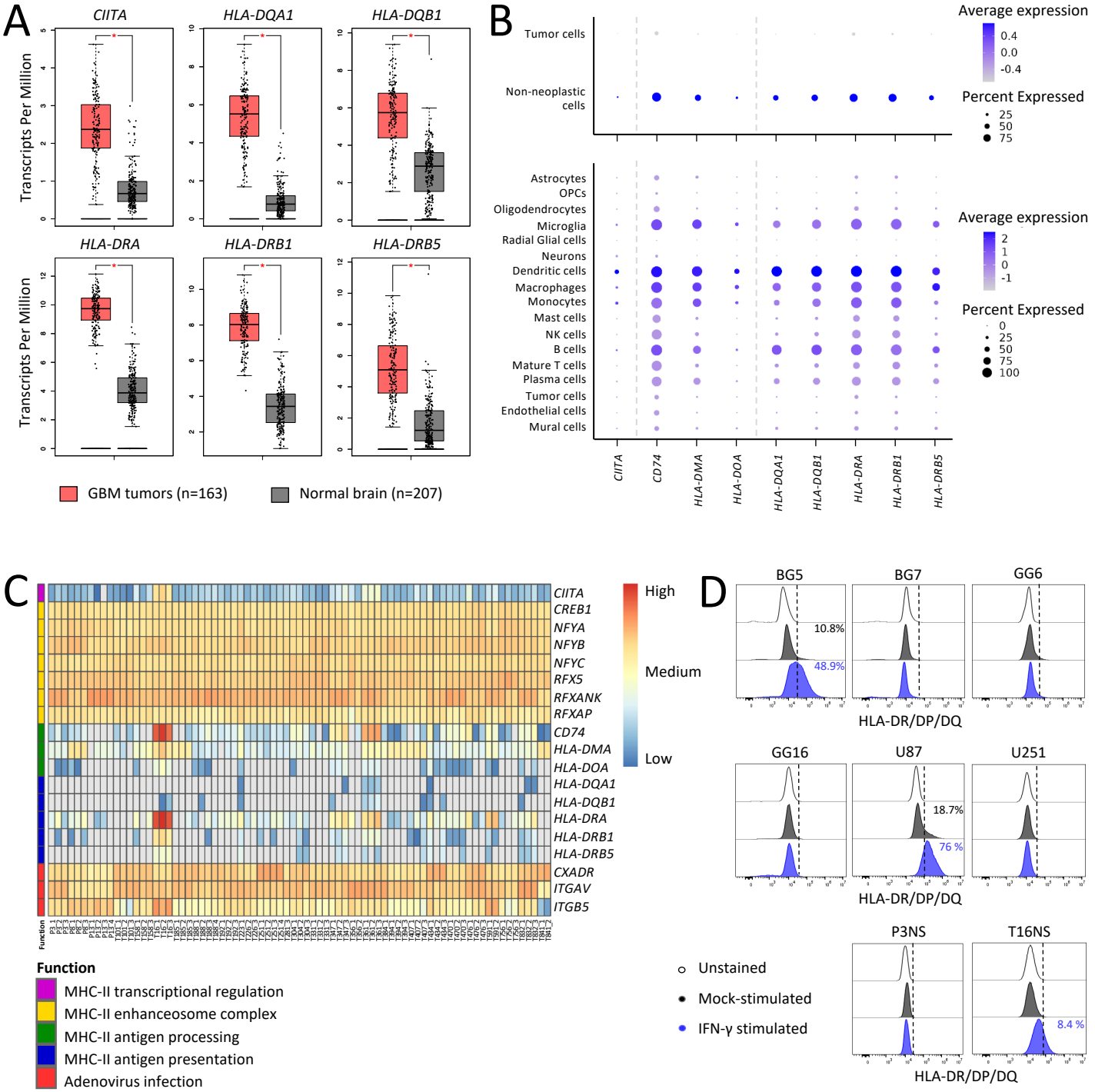
A
CIITA
HLA-DQA1
HLA-DQB1
HLA-DRA
HLA-DRB1
HLA-DRB5
Transcripts Per Million
GBM tumors (n=163)
Normal brain (n=207)
B
Tumor cells
Non-neoplastic cells
Astrocytes
OPCs
Oligodendrocytes
Microglia
Radial Glial cells
Neurons
Dendritic cells
Macrophages
Monocytes
Mast cells
NK cells
B cells
Mature T cells
Plasma cells
Tumor cells
Endothelial cells
Mural cells
CIITA
CD74
HLA-DMA
HLA-DOA
HLA-DQA1
HLA-DQB1
HLA-DRA
HLA-DRB1
HLA-DRB5
Average expression
Percent Expressed
C
CIITA
CREB1
NFYA
NFYB
NFYC
RFX5
RFXANK
RFXAP
CD74
HLA-DMA
HLA-DOA
HLA-DQA1
HLA-DQB1
HLA-DRA
HLA-DRB1
HLA-DRB5
CXADR
ITGAV
ITGB5
High
Medium
Low
Function
MHC-II transcriptional regulation
MHC-II enhanceosome complex
MHC-II antigen processing
MHC-II antigen presentation
Adenovirus infection
D
BG5
BG7
GG6
GG16
U87
U251
P3NS
T16NS
10.8%
48.9%
18.7%
76 %
8.4 %
HLA-DR/DP/DQ
Unstained
Mock-stimulated
IFN-γ stimulated

Figure 1

A

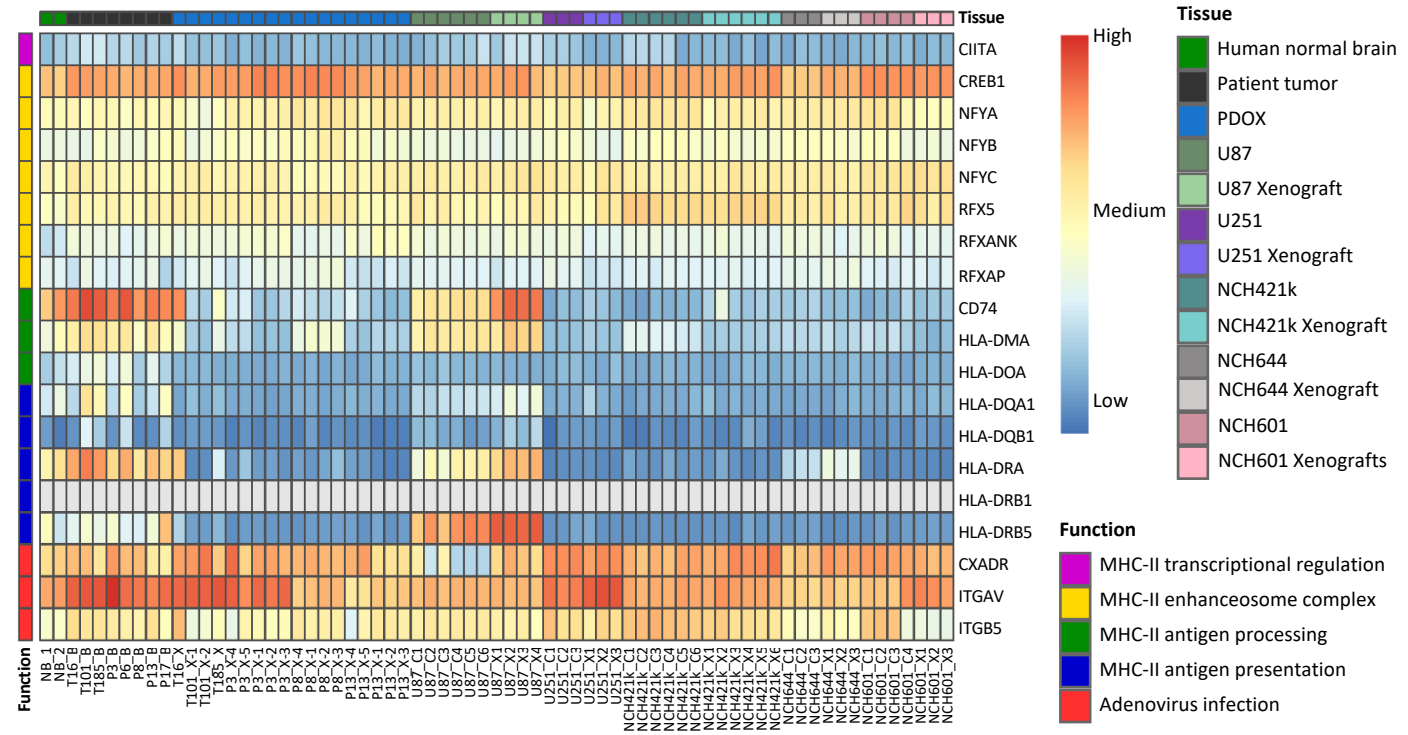

B

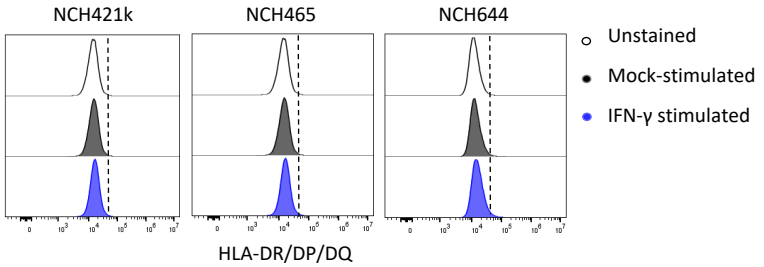

Supplementary Figure 1

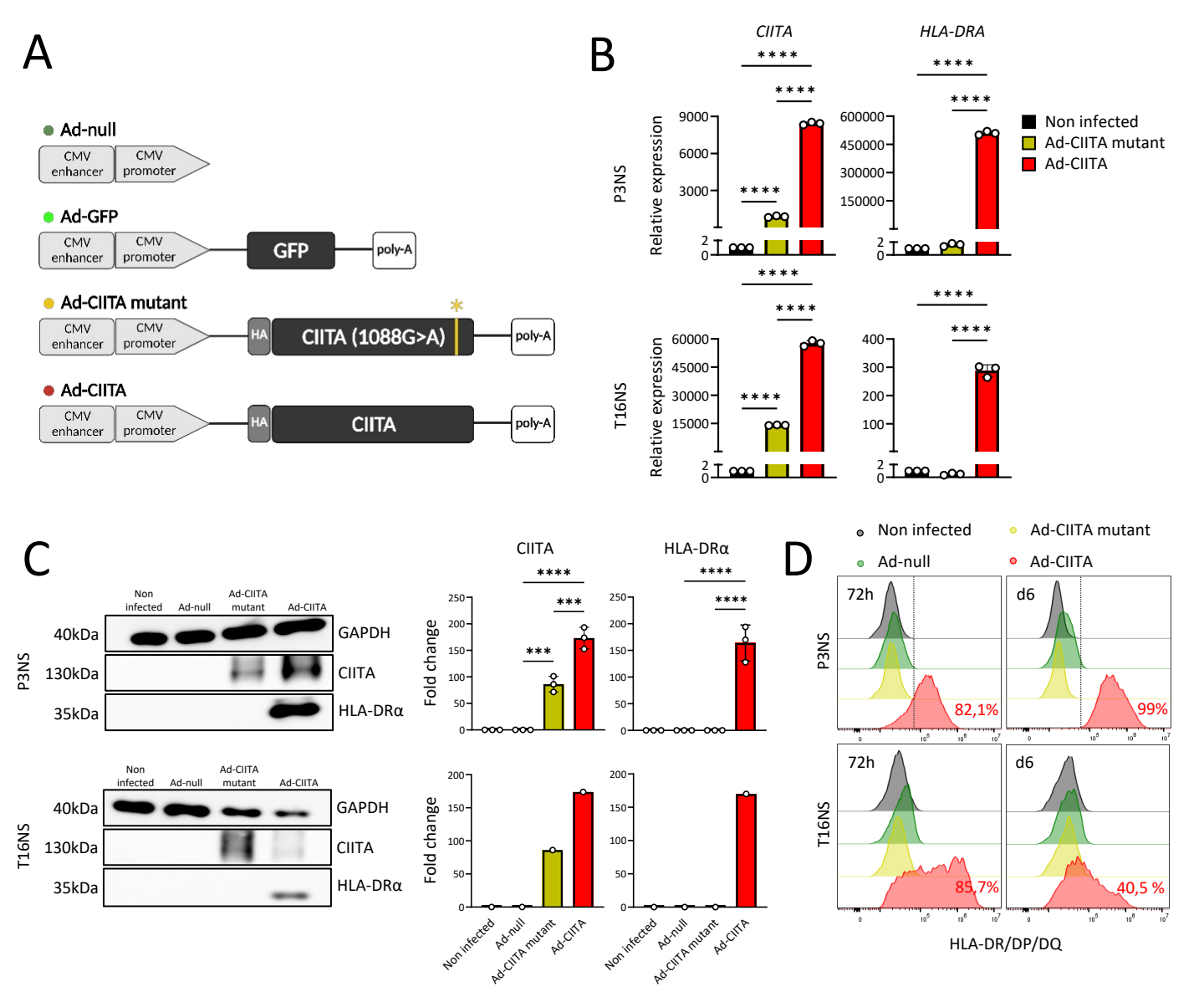
A
Ad-null
CMV enhancer
CMV promoter
Ad-GFP
GFP
poly-A
Ad-CIITA mutant
HA
CIITA (1088G>A)
Ad-CIITA
CIITA
B
CIITA
HLA-DRA
Relative expression
P3NS
T16NS
Non infected
Ad-CIITA mutant
Ad-CIITA
C
Non infected
Ad-null
Ad-CIITA mutant
Ad-CIITA
40kDa
130kDa
35kDa
GAPDH
CIITA
HLA-DRα
Fold change
HLA-DRα
D
Non infected
Ad-CIITA mutant
Ad-null
Ad-CIITA
72h
d6
82,1%
99%
85,7%
40,5 %
HLA-DR/DP/DQ

Figure 2

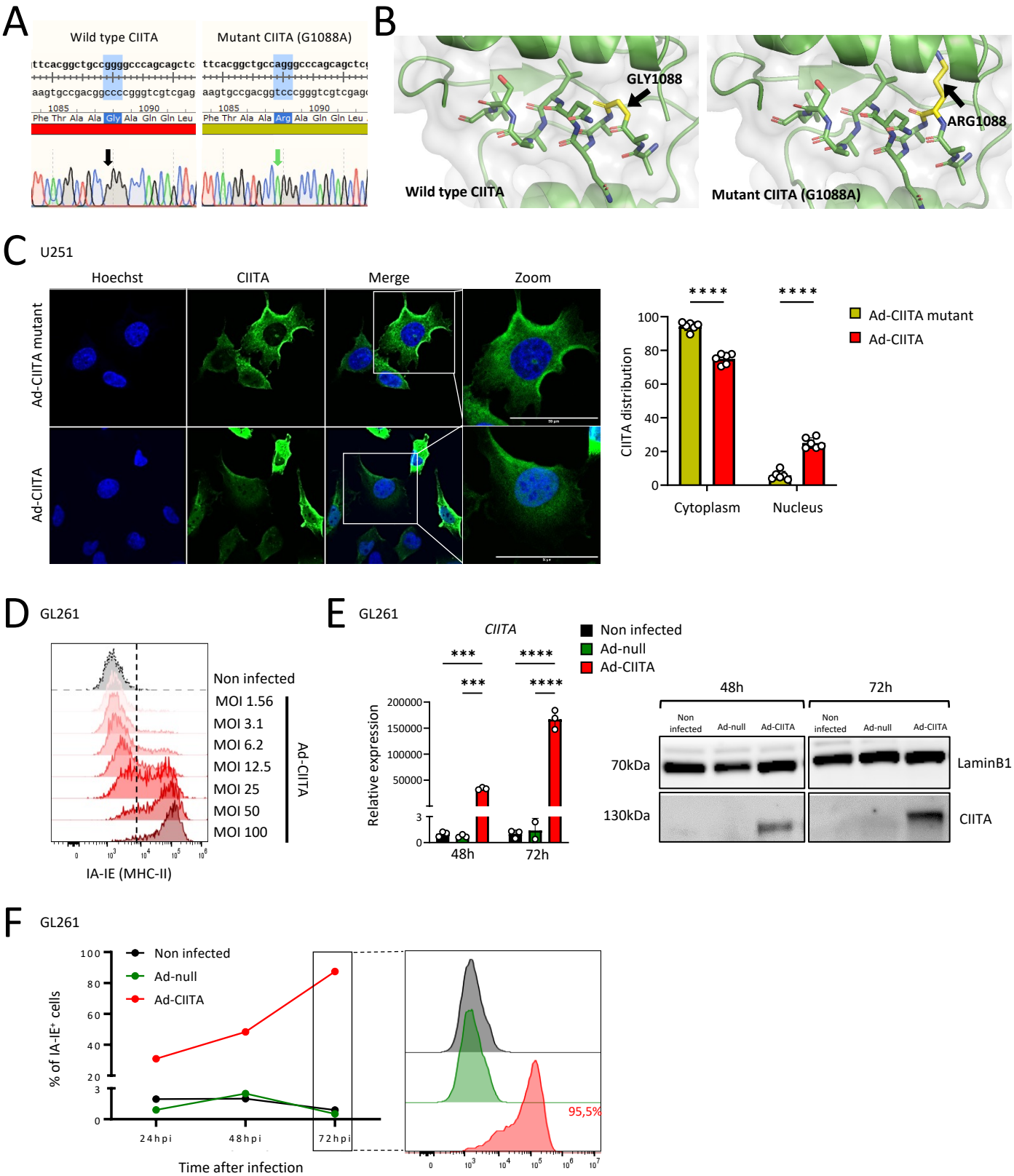

Supplementary Figure 2

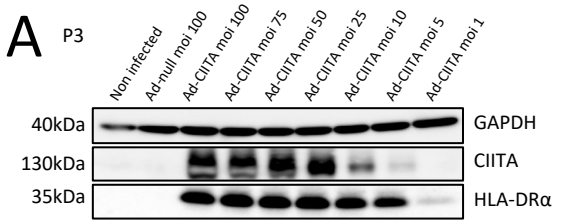
A
P3
Non infected
Ad-null moi 100
Ad-CIITA moi 100
Ad-CIITA moi 75
Ad-CIITA moi 50
Ad-CIITA moi 25
Ad-CIITA moi 10
Ad-CIITA moi 5
Ad-CIITA moi 1
40kDa
130kDa
35kDa
GAPDH
CIITA
HLA-DRα

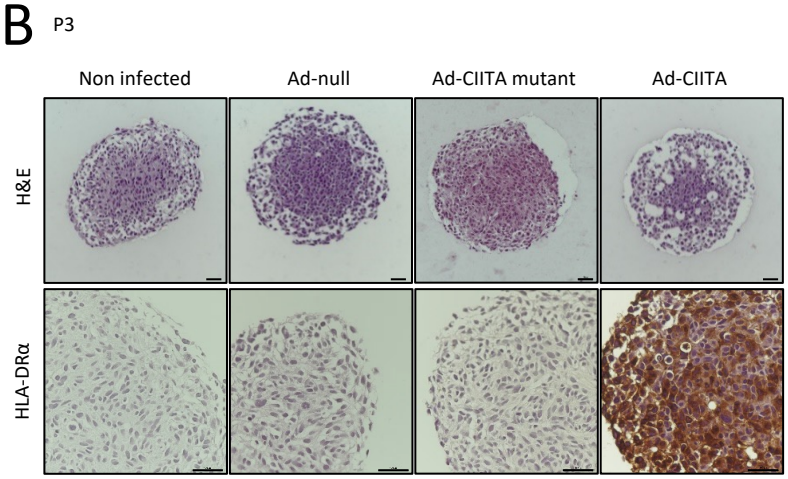
B
P3
Non infected
Ad-null
Ad-CIITA mutant
Ad-CIITA
H&E
HLA-DRα

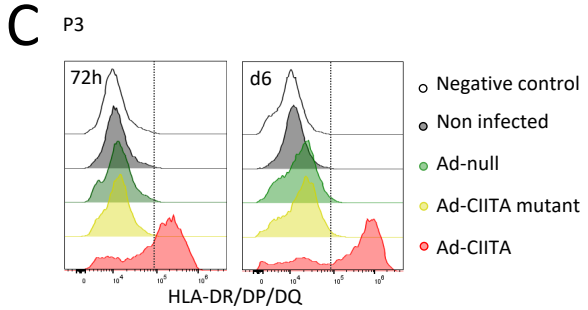
C
P3
72h
d6
Negative control
Non infected
Ad-null
Ad-CIITA mutant
Ad-CIITA
HLA-DR/DP/DQ

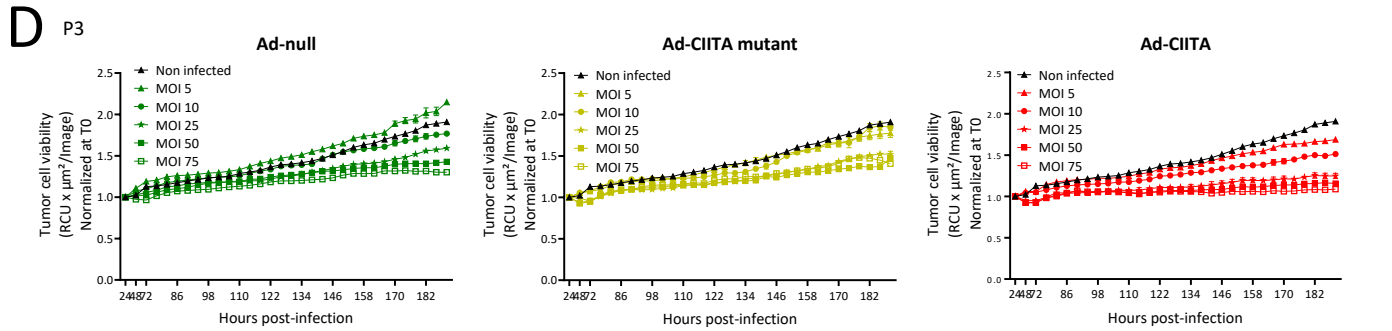
D
P3
Ad-null
Ad-CIITA mutant
Ad-CIITA
Non infected
MOI 5
MOI 10
MOI 25
MOI 50
MOI 75
Tumor cell viability
(RCU x µm²/Image)
Normalized at T0
Hours post-infection

Figure 3

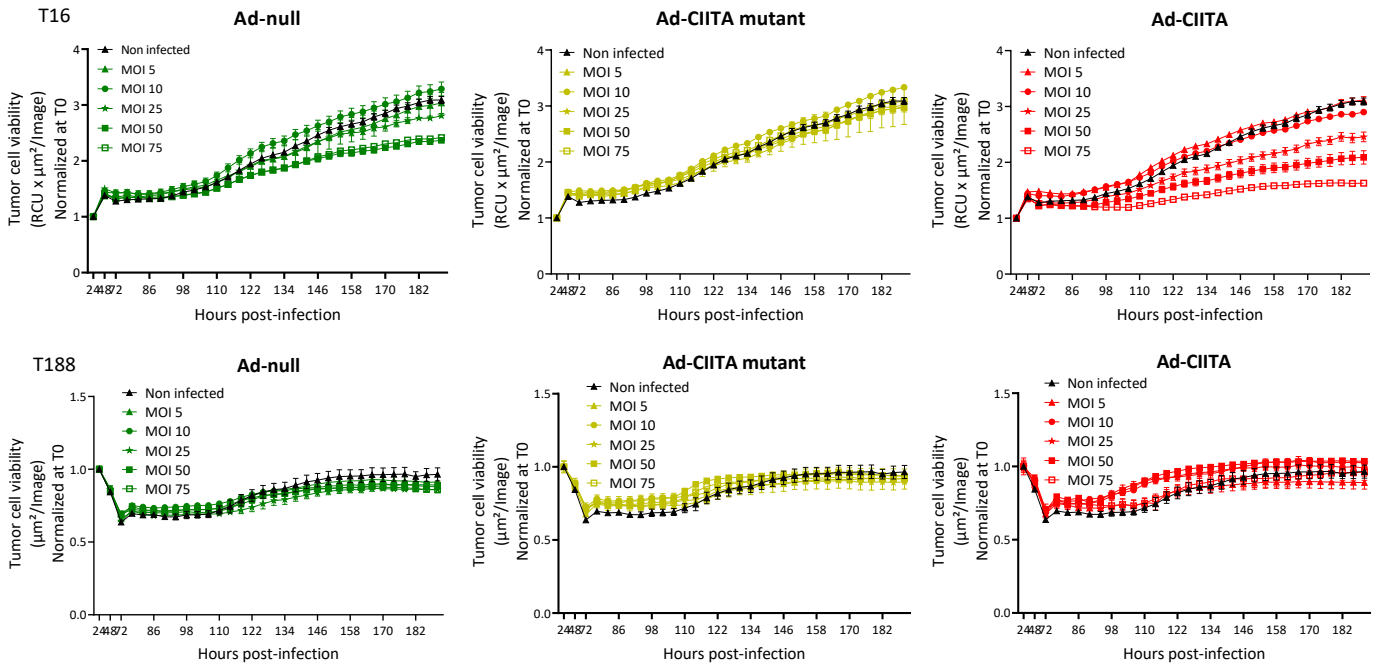

Supplementary Figure 3

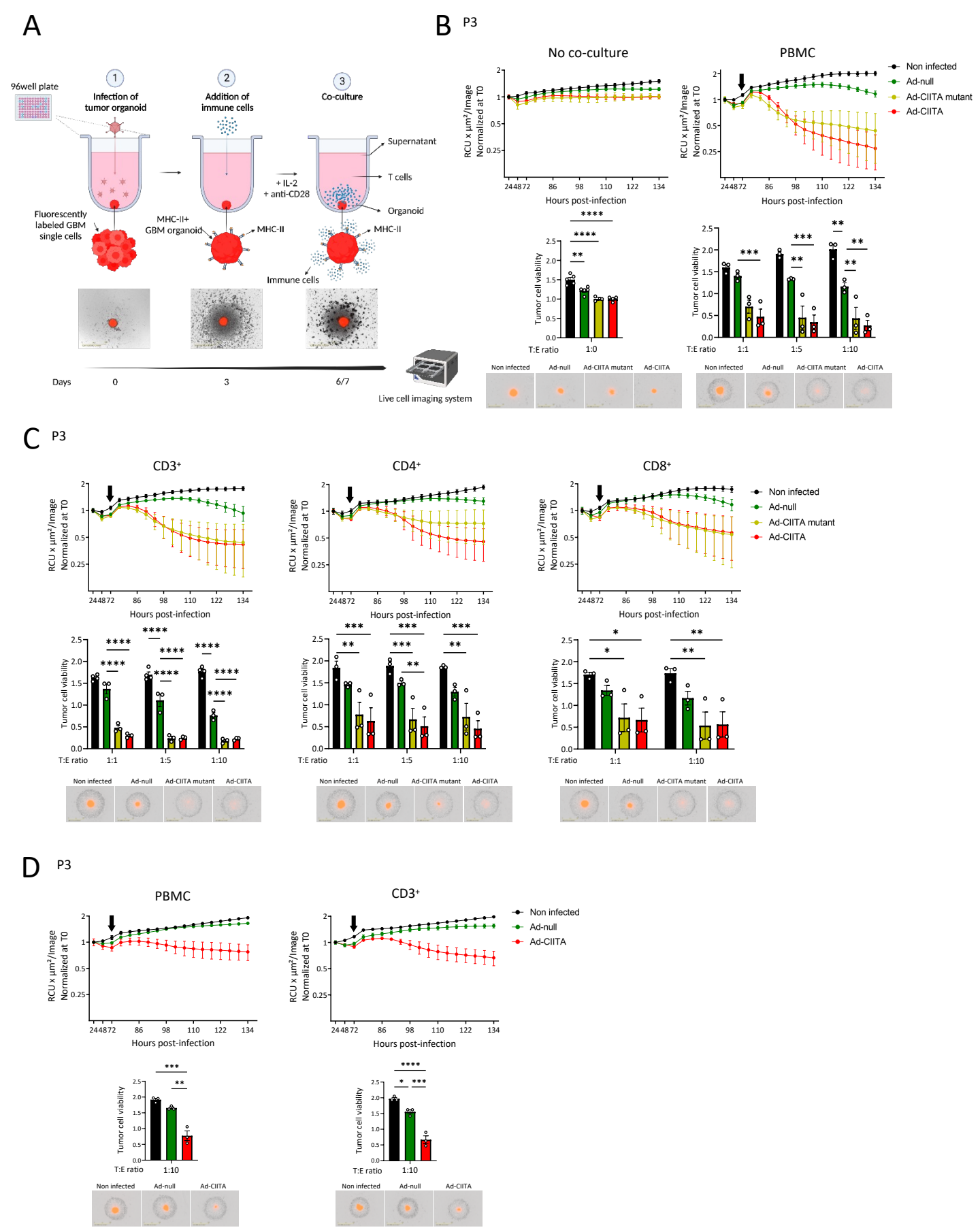
A
96well plate
1
Infection of tumor organoid
2
Addition of immune cells
3
Co-culture
Supernatant
T cells
+ IL-2
+ anti-CD28
Organoid
Fluorescently labeled GBM single cells
MHC-II+ GBM organoid
MHC-II
MHC-II
Immune cells
Days
0
3
6/7
Live cell imaging system
B
P3
No co-culture
PBMC
Non infected
Ad-null
Ad-CIITA mutant
Ad-CIITA
RCU x µm²/Image Normalized at T0
Hours post-infection
Tumor cell viability
T:E ratio
1:0
1:1
1:5
1:10
C
P3
CD3+
CD4+
CD8+
D
P3
PBMC
CD3+

Figure 4

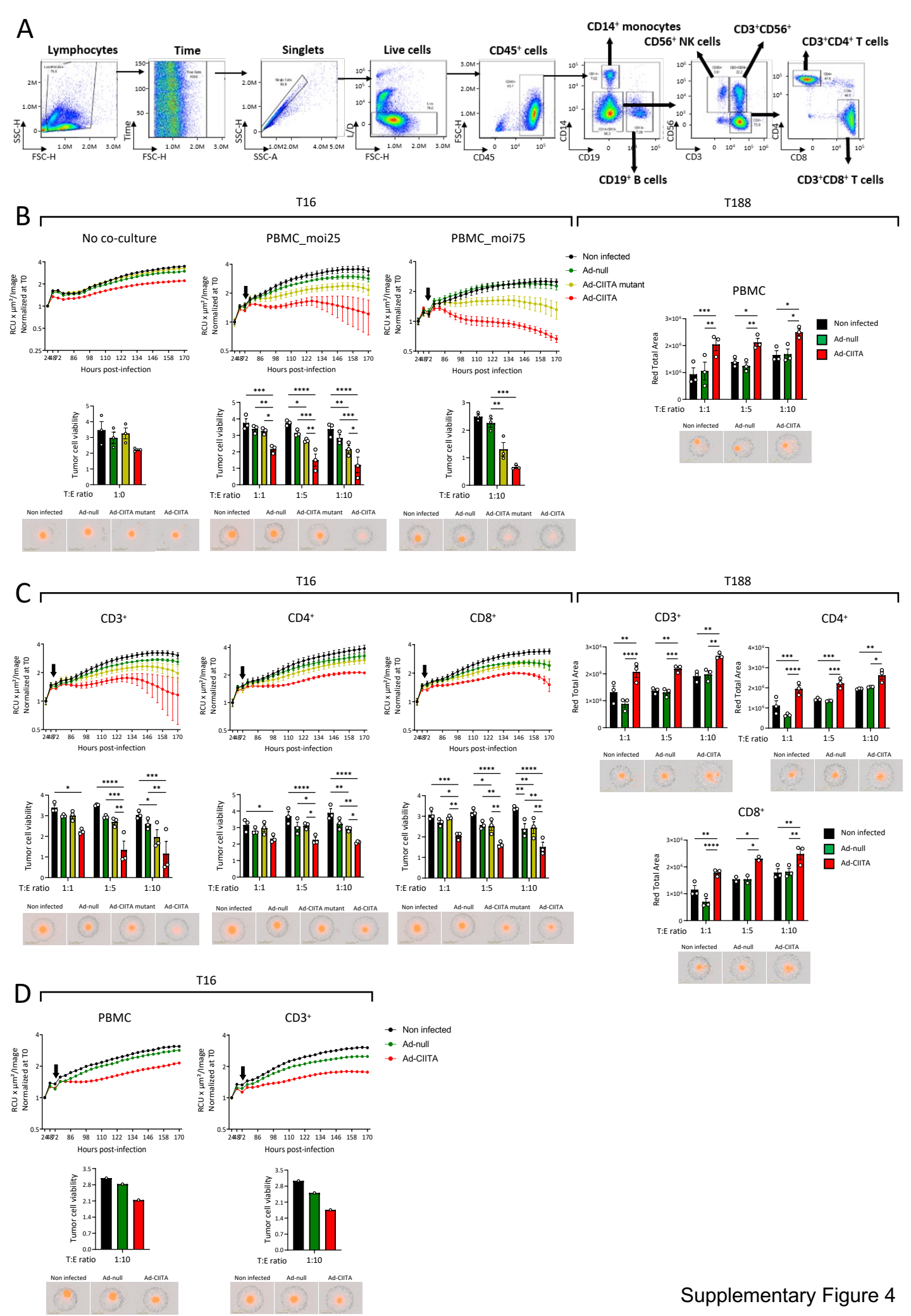

Supplementary Figure 4

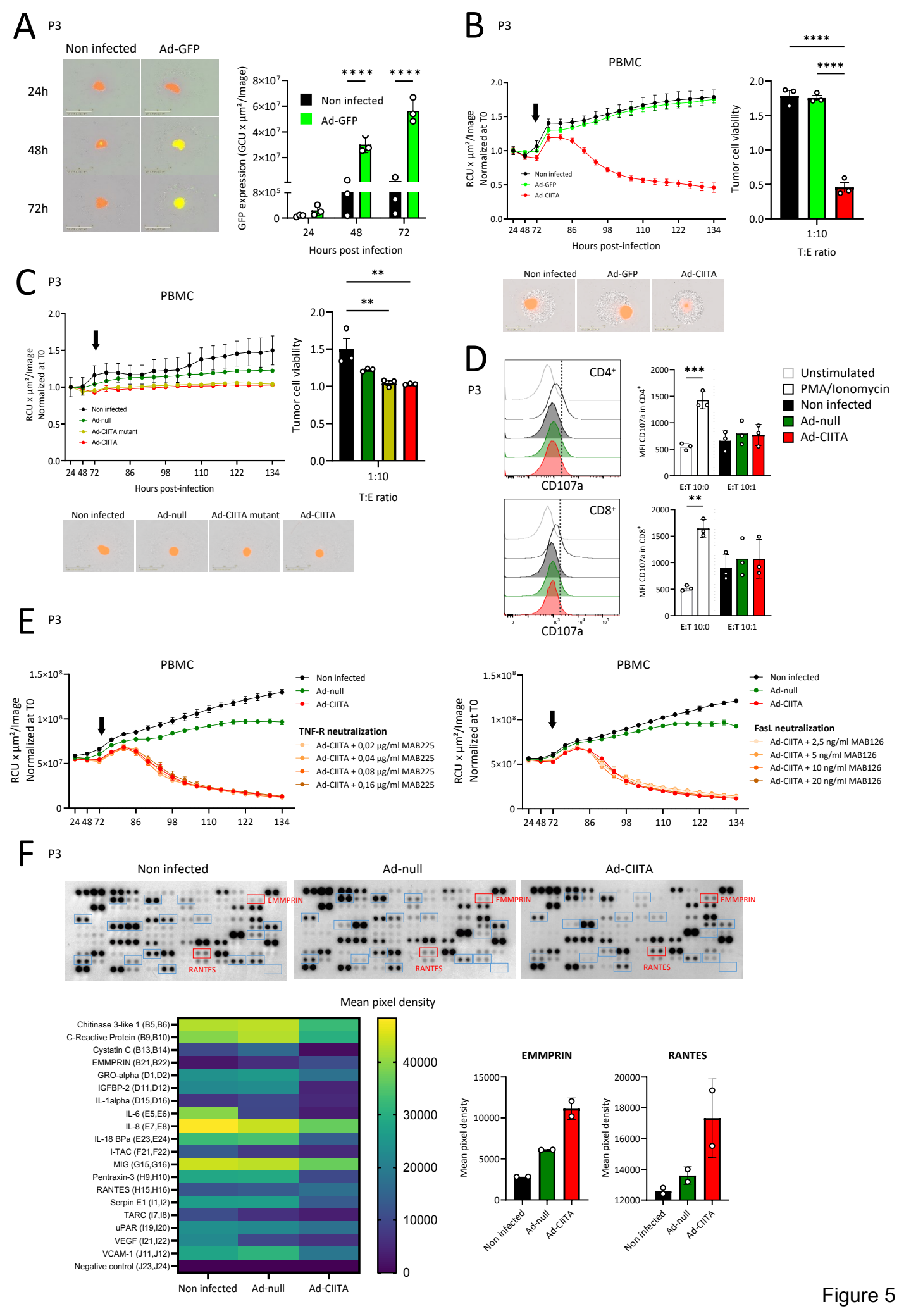
A
P3
Non infected
Ad-GFP
24h
48h
72h
GFP expression (GCU x µm²/Image)
Non infected
Ad-GFP
Hours post infection
B
P3
PBMC
RCU x µm²/Image Normalized at T0
Non infected
Ad-GFP
Ad-CIITA
Hours post-infection
Tumor cell viability
1:10
T:E ratio
C
P3
PBMC
Non infected
Ad-null
Ad-CIITA mutant
Ad-CIITA
D
P3
CD4+
CD8+
CD107a
MFI CD107a in CD4+
MFI CD107a in CD8+
E:T 10:0
E:T 10:1
Unstimulated
PMA/Ionomycin
Non infected
Ad-null
Ad-CIITA
E
P3
PBMC
TNF-R neutralization
Ad-CIITA + 0,02 µg/ml MAB225
Ad-CIITA + 0,04 µg/ml MAB225
Ad-CIITA + 0,08 µg/ml MAB225
Ad-CIITA + 0,16 µg/ml MAB225
FasL neutralization
Ad-CIITA + 2,5 ng/ml MAB126
Ad-CIITA + 5 ng/ml MAB126
Ad-CIITA + 10 ng/ml MAB126
Ad-CIITA + 20 ng/ml MAB126
F
P3
Non infected
Ad-null
Ad-CIITA
EMMPRIN
RANTES
Mean pixel density
Chitinase 3-like 1 (B5,B6)
C-Reactive Protein (B9,B10)
Cystatin C (B13,B14)
EMMPRIN (B21,B22)
GRO-alpha (D1,D2)
IGFBP-2 (D11,D12)
IL-1alpha (D15,D16)
IL-6 (E5,E6)
IL-8 (E7,E8)
IL-18 BPa (E23,E24)
I-TAC (F21,F22)
MIG (G15,G16)
Pentraxin-3 (H9,H10)
RANTES (H15,H16)
Serpin E1 (I1,I2)
TARC (I7,I8)
uPAR (I19,I20)
VEGF (I21,I22)
VCAM-1 (J11,J12)
Negative control (J23,J24)
EMMPRIN
RANTES

Figure 5

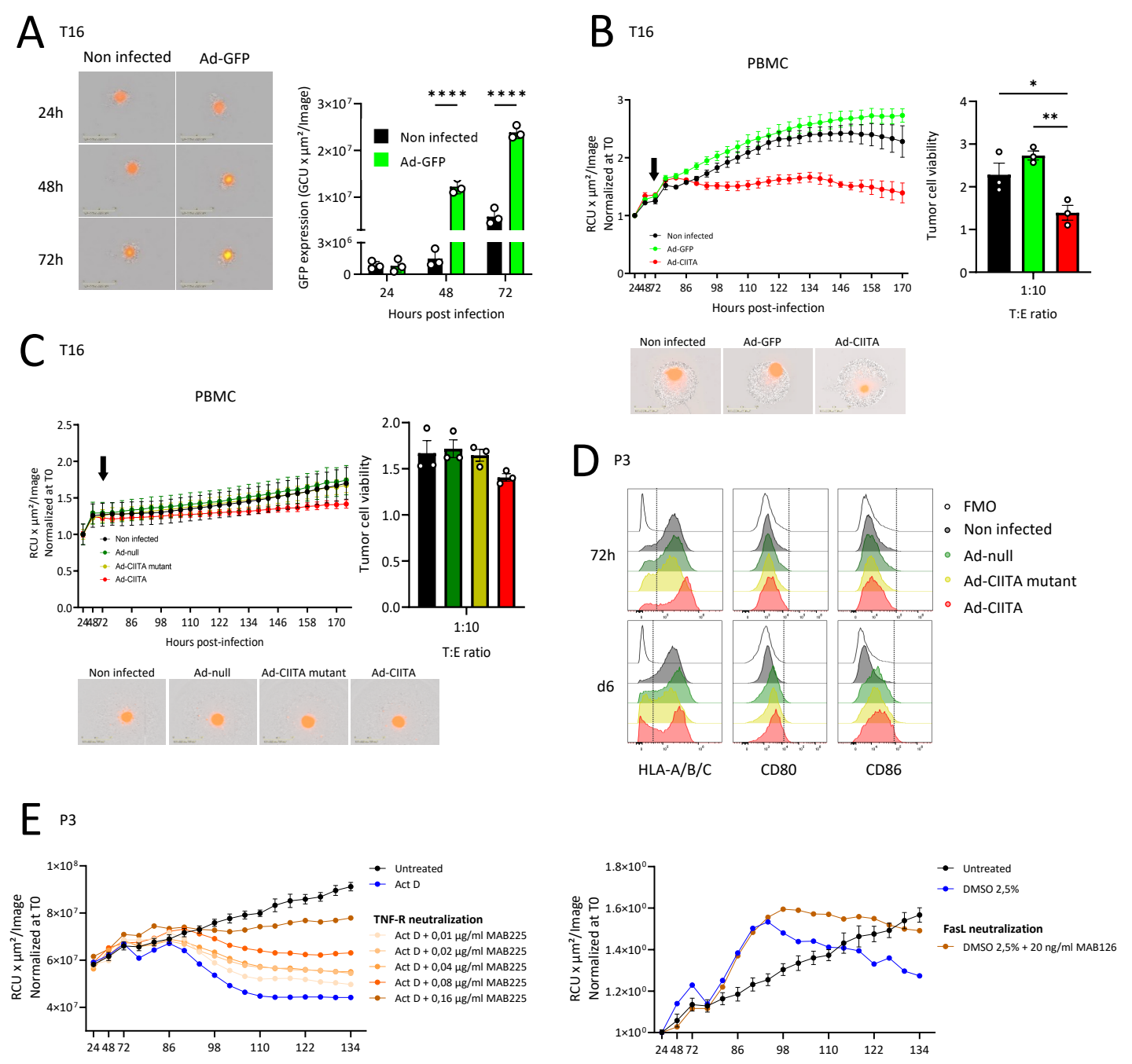

Supplementary Figure 5

Table S1. Molecular profiling of the PDOX models used in the study.

		Model		
		P3	**T16**	**T188**
Matched Patient information	Patient code	BER0003	LIH0016	LIH0188
	Age at collection	64	52	68
	Sex	Male	Female	Male
	Tumor localization	N/A	Fronto-parietal right	N/A
	Surgery	N/A	Recurrence	Primary
	Treatment received prior PDOX	N/A	TMZ	No prior treatment
	Histological diagnosis	GBM Grade IV	GBM Grade IV	GBM Grade IV
PDOX characteristics	Original stain of mouse	NOD.CB17-Prkdc^{scid}/J	NOD.CB17-Prkdc^{scid}/J	NOD.CB17-Prkdc^{scid}/J
	Site of implantation	Brain	Brain	Brain
	Implantation	Organoids	Organoids	Organoids
	PDOX survival time (days)	42.5 +/- 3.6	75 +/- 6.5	64 +/- 10
	Proliferation index in PDOX (% Ki67 +/- SD)	54.7 +/- 3.7	18.9 +/- 5.8	37.1+/- 2.9
	Ploidy PDOX	2.1N	(2.1N) + 3.4N	2.3N
Molecular features in PDOXs	Copy number variations (CNV)	+[Chr7, 19p, 20q], -[1p36-1p34.1, 1q21.1-q44, -5p15.33-31, Chr9, Chr10, 11p15-14, 20p] --CDKN2A/B	++[EGFR, MDM4], +7q, - [6q, Chr10, 13q11-q31.1], --CDKN2A/B	[++EGFR], +[Chr7, Chr 19, Chr 20], -[1p36.23, 6p21.32, 6q27, Chr 10, 11q24.2], --CDKN2A/B
	Glioma-specific gene mutations	PTEN (chr10:g.87957923del, ENSP00000361021.3:p.Asp236ThrfsTer20) TP53 (chr17:g.7675085C>T, ENSP00000269305.4:p.Cys176Tyr)	EGFR ex25-27del	EGFR ex-6-7del, ex25-26del, MDM4 (chr1:g.204549329A>C, ENSP00000356150.3:p.Lys374Gln) PTCH1 (chr9:g.95459693C>T, ENSP00000332353.6:p.Val932Ile)
	DNA methylation profiles	GBM, IDHwt, RTK II	GBM, IDHwt, RTK II	GBM, IDHwt, RTK II/I
	MGMT promoter methylation	Methylated	Unmethylated	Unmethylated
	Verhaak glioma subtypes classification	Classic-like	Classical	Classic-like

Table S2. Composition of PBMC and isolated sub-populations before co-culture (shown as % of CD45+).

CR014	**% CD14⁺**	**% CD19⁺**	**% CD3⁺**	**% CD4⁺**	**% CD8⁺**	**% CD56⁺**
PBMC	29,9 ± 0,64	3,72 ± 0,28	49 ± 1,56	38,2 ± 1,41	8,68 ± 0,25	5,5 ± 0,06
Isolated CD3⁺	0,39 ± 0,06	0,12 ± 0,01	91,33 ± 1,23	70,73 ± 1,39	16,47 ± 0,14	0,2 ± 0,05
Isolated CD4⁺	0,02 ± 0,01	0,01 ± 0	98,2 ± 0,58	96,37 ± 1,02	0,02 ± 0,01	0,01 ± 0
Isolated CD8⁺	0,04 ± 0,02	0,01 ± 0	92,47 ± 1,93	0,48 ± 0,37	84,67 ± 3,84	0,04 ± 0,01

CR015	**% CD14⁺**	**% CD19⁺**	**% CD3⁺**	**% CD4⁺**	**% CD8⁺**	**% CD56⁺**
PBMC	20,2 ± 1,04	3,6 ± 0,33	61,33 ± 4,86	41,67 ± 2,26	18,03 ± 2,34	6 ± 0,03
Isolated CD3⁺	0,295 ± 0,1	0,049 ± 0,01	93,8 ± 1,83	66,53 ± 1,09	24 ± 3,07	0,42 ± 0,09
Isolated CD4⁺	0,02 ± 0,01	0,01 ± 0	99,27 ± 0,15	96,9 ± 0,41	0,61 ± 0,47	0,01 ± 0
Isolated CD8⁺	0,1 ± 0,05	0,03 ± 0,01	96,63 ± 1,16	1,23 ± 1,59	90,07 ± 3,64	0,02 ± 0,01

CR017	**% CD14⁺**	**% CD19⁺**	**% CD3⁺**	**% CD4⁺**	**% CD8⁺**	**% CD56⁺**
PBMC	6.85	7.2	61.8	29.5	29.8	3.05
Isolated CD3⁺	0.03	0.03	90.40	43.90	42.7	0.086
Isolated CD4⁺	0.01	0.03	98.80	92.30	4.17	0.00168
Isolated CD8⁺	0.01	0.01	96.30	0.01	94.2	0.011

CTL500	**% CD14⁺**	**% CD19⁺**	**% CD3⁺**	**% CD4⁺**	**% CD8⁺**	**% CD56⁺**
PBMCs	27.3	3.65	52.4	28.8	18.7	7.51
Isolated CD3⁺	0.11	0.034	93.7	50.6	34.6	1.44

CTL573	**% CD14⁺**	**% CD19⁺**	**% CD3⁺**	**% CD4⁺**	**% CD8⁺**	**% CD56⁺**
PBMC	21.6	6.29	61.5	33.9	24.5	4.53
Isolated CD3⁺	0.66	0.18	92	51.2	35.2	2.49

CTL640	**% CD14⁺**	**% CD19⁺**	**% CD3⁺**	**% CD4⁺**	**% CD8⁺**	**% CD56⁺**
PBMC	14.9	3.38	56.2	38.9	14.7	14.1
Isolated CD3⁺	0.14	1.50E-01	86.4	59.8	21.8	6.92

Table S3. Tumor/Immune cells typing at MHC-I and MHC-II loci.

P3 tumor		Tumor cells	Immune cells					
		P3	CTL573	CTL500	CTL640	CR014	CR015	CR017
MHC-I	HLA-A	2:01:01	2:01	1:01	2:01	N/A	N/A	N/A
		~	3:01	2:01	29:02:00	N/A	N/A	N/A
	HLA-B	27:05:02G	7:02	44:02:00	39:01:00	N/A	N/A	N/A
		44:02:01G	44:02:00	57:01:00	44:02:00	N/A	N/A	N/A
	HLA-C	1:02:01	5:01	5:01	5:01	N/A	N/A	N/A
		5:01:01	7:02	6:02	12:03	N/A	N/A	N/A
MHC-II	HLA-DRB1	4:01:01	4:01	4:01	4:01	N/A	N/A	N/A
		4:08:01	15:01	13:05	11:01	N/A	N/A	N/A
	HLA-DQB1	3:01:01	3:01	3:01	3:01	N/A	N/A	N/A
		~	6:02	3:01	~	N/A	N/A	N/A
	HLA-DPB1	2:01:02	4:01	04:01G	4:01	N/A	N/A	N/A
		4:01:01	11:01	04:01G	23:01	N/A	N/A	N/A
	HLA-DQA1	3:03:01	1:02	not tested	3:01	N/A	N/A	N/A
		~	3:01	not tested	5:01	N/A	N/A	N/A
	HLA-DRB3/4/5	DRB4*01:03:01	DRB4*01:01	DRB3*02:02	DRB3*02:02	N/A	N/A	N/A
		~	DRB5*01:01	DRB4*01:03	DRB4*01:01	N/A	N/A	N/A
	HLA-DPA1	1:03:01	1:03	1:03	1:03	N/A	N/A	N/A
		~	2:01	1:03	~	N/A	N/A	N/A
		Match	7/9	8/9	7/9	0/9	0/9	0/9

T16 tumor		Tumor cells	Immune cells			
		T16	CTL572	CR014	CR015	CR017
MHC-I	HLA-A	2:01:01	2:01	N/A	N/A	N/A
		68:02:01	3:01:00	N/A	N/A	N/A
	HLA-B	8:01:01	7:02:00	N/A	N/A	N/A
		35:01:01G	8:01	N/A	N/A	N/A
	HLA-C	4:01:01	7:01	N/A	N/A	N/A
		7:01:01	7:02	N/A	N/A	N/A
MHC-II	HLA-DRB1	03:01:01G	3:01	N/A	N/A	N/A
		11:01:01G	15:01	N/A	N/A	N/A
	HLA-DQB1	2:01:01	2:01	N/A	N/A	N/A
		3:01:01	6:02	N/A	N/A	N/A
	HLA-DPB1	1:01:01	2:01	N/A	N/A	N/A
		4:01:01	4:01	N/A	N/A	N/A
	HLA-DQA1	5:01:01	1:02	N/A	N/A	N/A
		5:05:01	5:01	N/A	N/A	N/A
	HLA-DRB3/4/5	DRB3*01:01:02G	DRB3 01:01	N/A	N/A	N/A
		DRB3*02:02:01	DRB5 01:01	N/A	N/A	N/A
	HLA-DPA1	1:03:01	1:03	N/A	N/A	N/A
		2:01:02	~	N/A	N/A	N/A
		Match	9/9	0/9	0/9	0/9

T188 tumor		Tumor cells	Immune cells		
		T188	CR014	CR015	CR017
MHC-I	HLA-A	2:01:01	N/A	N/A	N/A
		3:01:01	N/A	N/A	N/A
	HLA-B	7:02:01	N/A	N/A	N/A
		15:01:01G	N/A	N/A	N/A
	HLA-C	1:02:01	N/A	N/A	N/A
		7:02:01	N/A	N/A	N/A
MHC-II	HLA-DRB1	15:01:01	N/A	N/A	N/A
		13:01:01	N/A	N/A	N/A
	HLA-DQB1	6:02:01	N/A	N/A	N/A
		6:03:01	N/A	N/A	N/A
	HLA-DPB1	4:01:01	N/A	N/A	N/A
		13:01:01G	N/A	N/A	N/A
	HLA-DQA1	1:02:01	N/A	N/A	N/A
		1:03:01	N/A	N/A	N/A
	HLA-DRB3/4/5	DRB3*02:02:01	N/A	N/A	N/A
		DRB5*01:01:01	N/A	N/A	N/A
	HLA-DPA1	1:03:01	N/A	N/A	N/A
		2:01:04	N/A	N/A	N/A
		Match	0/9	0/9	0/9

~ Homozygous

G ambigous allele typing

Table S4. List of all antibodies used in the study.

Antibody	Fluorochrome	Clone	Application	Dilution	Incubation	Vendor	Cat. No.
CIITA	-	7-1H	WB/IF	1:200	O/N at 4°C	Santa Cruz	sc-13556
Alexa Fluor 488	-	Polyclonal	IF	1:10000	1 hour at RT	ThermoFisher	A11001
CD107a	BV785	H4A3	FACS	1:20	30 min at 4°C	BioLegend	328644
CD11b	BV785	ICRF44	FACS	1:20	30 min at 4°C	Biolegend	301346
CD14	PE-Cy7	63D3	FACS	1:20	30 min at 4°C	Biolegend	367112
CD19	BB770	SJ25C1	FACS	1:20	30 min at 4°C	BD Biosciences	566396
CD3	BV510	UCHT1	FACS	1:20	30 min at 4°C	BioLegend	300448
CD4	PE-Cy5	RPA-T4	FACS	1:166	30 min at 4°C	BioLegend	300510
CD45	FITC	2D1	FACS	1:20	30 min at 4°C	BioLegend	368508
CD56	PE-Dazzle CF594	NCAM16.2	FACS	1:166	30 min at 4°C	BD Biosciences	564849
CD8	APC	RPA-T8	FACS	1:60	30 min at 4°C	BioLegend	301014
CD80	PE	L307.4	FACS	1:5	30 min at 4°C	BD Biosciences	560925
CD86	BV421	2331 (FUN-1)	FACS	1:20	30 min at 4°C	BD Biosciences	562433
Fas Ligand/TNFSF6	-	100419	Neutralization	-	-	R&D systems	MAB126
GAPDH	-	D16H11	WB	1:10000	O/N at 4°C	Cell Signalling	5174S
HLA-A,B,C	BV510	W6/32	FACS	1:20	30 min at 4°C	BioLegend	311435
HLA-DR	-	EPR3692	IHC	1:200	3 hour at RT	Abcam	ab92511
HLA-DR,DP,DQ	FITC	Tu39	FACS	1:5	30 min at 4°C	BD Biosciences	555558
HLA-DRα	-	G-7	WB	1:100	O/N at 4°C	Santa Cruz	sc-55593
Hoechst 33258	-	-	IF	1:10000	1 hour at RT	ThermoFisher	H3569
HRP secondary	-	Polyclonal	WB	1:10000	1 hour at RT	Jackson ImmunoResearch	111-035-003
I-A/I-E	PerCP/Cy5.5	M5/114.15.2	FACS	1:40	30 min at 4°C	BioLegend	107626
Lamin B1	-	Polyclonal	WB	1:10000	O/N at 4°C	Abcam	ab16048
Live/Dead fixable Near-IR	APC-Cy7	-	FACS	1:1000	30 min at 4°C	Invitrogen	L34975
TNF RI/TNFRSF1A	-	16803	Neutralization	-	-	R&D systems	MAB225